Contributions to Mineralogy and Petrology (2020) 175:25
https://doi.org/10.1007/s00410-020-1655-6

ORIGINAL PAPER

The origin of low-MgO eclogite xenoliths from Obnazhennaya kimberlite, Siberian craton

Jing Sun[1,2] · Roberta L. Rudnick[3] · Sergey Kostrovitsky[4,5] · Tatiana Kalashnikova[4] · Kouki Kitajima[6] · Ranpeng Li[3] · Qiao Shu[7,8]

Received: 11 August 2019 / Accepted: 11 January 2020 / Published online: 21 February 2020

Abstract

The petrology, mineral major and trace-element concentrations, and garnet oxygen isotopic composition of low-MgO (11–16 wt%) eclogites from the Obnazhennaya kimberlite, Siberian craton, are used to infer their petrogenesis. These eclogites contain two types of compositionally distinct garnet: granular coarse garnet, and garnet exsolution (lamellae and fine-grained garnet) in clinopyroxene. The former record higher temperatures at lower pressures than the latter, which record the last stage of equilibrium at moderate pressure–temperature conditions 2.3–3.7 GPa and 855–1095 °C in the upper mantle at the time of entrainment. Although derived from the garnet stability field, these rocks have low-pressure cumulate protoliths containing plagioclase, olivine, and clinopyroxene as reflected by pronounced positive Eu and Sr anomalies in all eclogites, and low heavy rare earth element (HREE) contents in both minerals and reconstructed bulk rocks for a number of samples. Major elements, transition metals, and the HREE compositions of the reconstructed whole rocks are analogous to modern oceanic gabbro cumulates. Despite geochemical signatures supporting an oceanic crust origin, mantle-like $\delta^{18}O$ of the garnets (5.07–5.62‰) for most samples indicates that the protoliths either did not interact with seawater or have coincidently approximately normal igneous values. Some of the eclogite xenoliths have lower SiO_2 contents and depleted light REE ($(Nd/Yb)_N < 1$) compared to modern oceanic gabbros, suggesting that they experienced partial melting. Positively inclined middle to heavy REE patterns ($(Dy/Yb)_N < 1$) of the reconstructed bulk rocks mostly result from repeated partial melting in the eclogite stability field, based on melting model calculations. We, therefore, suggest that the Obnazhennaya low-MgO eclogites may represent the gabbroic section of subducted or foundered basaltic crust that underwent continued partial melting processes at high pressures, where garnet was the main residual phase.

Keywords Obnazhennaya · Low-MgO eclogite xenolith · Low-pressure origin · Garnet exsolution · Cumulates

Electronic supplementary material The online version of this article (https://doi.org/10.1007/s00410-020-1655-6) contains supplementary material, which is available to authorized users.

✉ Jing Sun
sunjingvv@163.com

✉ Qiao Shu
shuqiao@mail.gyig.ac.cn

[1] State Key Laboratory of Petroleum Resources and Engineering, Beijing 102249, China

[2] College of Geosciences, China University of Petroleum (Beijing), Beijing 102249, China

[3] Department of Earth Science and Earth Research Institute, University of California, Santa Barbara, CA 93106, USA

[4] Institute of Geochemistry, Siberian Branch of the Russian Academy of Sciences, 664033 Irkutsk, Russia

[5] Institute of Earth Crust, Siberian Branch of the Russian Academy of Sciences, 664033 Irkutsk, Russia

[6] Department of Geoscience, University of Wisconsin-Madison, Madison, WI 53706, USA

[7] State Key Laboratory of Ore Deposit Geochemistry, Institute of Geochemistry, Chinese Academy of Sciences, Guiyang 550081, China

[8] CAS Center for Excellence in Comparative Planetology, Hefei, China

Introduction

Eclogite is a volumetrically small (< 1%), but important and integral part of the continental lithosphere (Schulze 1989). Xenolithic eclogites exhibit a broad compositional spectrum (Aulbach and Jacob 2016), and their origins could vary accordingly. Several possible origins have been proposed for xenolithic eclogites: (1) cumulates of mantle melt formed at high pressure (e.g., O'Hara 1969); (2) residues of melted subducted oceanic crust (e.g., Ireland et al. 1994; Jacob and Foley 1999; Barth et al. 2001); (3) subducted low-pressure cumulates (e.g., Barth et al. 2002; Shu et al. 2016); and (4) products of melt-rock reaction (e.g., Smart et al. 2009; Wang et al. 2015). Due to their possible origin via ancient subduction, eclogites may hold clues to the past thermal, redox, and chemical state of the ambient convecting mantle (e.g., Aulbach and Stagno 2016; Aulbach and Arndt 2019). Hence, it is important to characterize eclogite xenoliths geochemically to place better constraints on their origins, and the implications for the operation of major earth processes in the past.

Eclogites with low bulk rock MgO contents are generally interpreted to originate as subducted oceanic crust. Examples include low-MgO eclogite xenoliths from South Africa (e.g., Gréau et al. 2011; Huang et al. 2012; Huang et al. 2014; Shu et al. 2013), Finland (Peltonen et al. 2002), West Africa (e.g., Barth et al. 2001; Aulbach et al. 2019), Slave craton, Canada (e.g., Aulbach et al. 2007; Smart et al. 2012) and from Udachnaya pipe in the middle of the Siberian craton (Agashev et al. 2018; and references therein). A further important locality for eclogite and pyroxenite xenoliths, the non-diamondiferous Obnazhennaya kimberlite, is located on the northeastern edge of the Siberian craton. These xenoliths can provide information on the shallower lithosphere evolution history of this region, and provide information about processes occurring at the edge of the platform.

Eclogite or pyroxenite xenoliths from the Obnazhennaya kimberlite pipe can be divided into two broad groups based on their petrological characteristics. One group of samples is bimineralic, composed of garnet and clinopyroxene containing lamellae-shaped garnet exsolutions; they were named Group B/C eclogites in previous studies (Taylor et al. 2003) according to their garnet composition. The MgO content of reconstructed bulk rocks of this group is always lower than 16%, and we call this group "low-MgO eclogites". The other group of samples, previously named Group A eclogites (Qi et al. 1994; Taylor et al. 2003; Alifirova et al. 2012, 2015) or websterites (Spengler and Alifirova 2019), contain minor orthopyroxene and rutile in addition to garnet and clinopyroxene. This group of samples has higher MgO content in the reconstructed bulk rock, and is referred to as "high-MgO" here. A large number of high-MgO eclogites and pyroxenites from Obnazhennaya have previously been studied (Qi et al. 1994; Taylor et al. 2003; Alifirova et al. 2012, 2015). However, far fewer studies have been carried out on the Obnazhennaya low-MgO eclogites.

The eclogite xenoliths invested here contain both granular garnet and garnet exsolutions in host clinopyroxenes, which allows us to place constraints not only on their origin and evolution but also the thermal state of the lithospheric mantle beneath the margin of the Siberian craton. In this paper, we present new major, trace element, and oxygen-isotope results for eight fresh low-MgO Obnazhennaya eclogites. We integrate our new data with the previously published data for three Group B eclogites from this pipe (Taylor et al. 2003) to decipher their origins and garnet exsolution history.

Geological setting and prior work

The Siberian platform extends more than 2500 km from Lake Baikal in the south to the Arctic Ocean in the north, and from the Yenisey River in the west to the Aldan shield in the east (Fig. 1). Moho depths beneath the platform range from 35 to 60 km (Rosen et al. 1994). Phanerozoic kimberlites with ages from 420 to 150 Ma (Sun et al. 2014) erupted within the region marked "Yakutian kimberlite Province" in Fig. 1. The Obnazhennaya kimberlite pipe lies within the Kuoika field, which occupies the extreme northeastern portion of the platform (Fig. 1). The age of the Obnazhennaya kimberlite is not well defined. Zircon and perovskite U–Pb dates from other pipes in the Kuoika field range from 156 to 167 Ma (Davis et al. 1980; Kinny et al. 1997; Blanco et al. 2013; Sun et al. 2014). Paleomagnetic studies of the Obnazhennaya pipe suggest an age of 168 Ma (Blanco et al. 2013). Therefore, ~ 160 Ma is assumed to be the eruption age of this pipe (Smelov and Zaitsev 2013).

We collected a suite of fresh samples and chose those without orthopyroxene and with low MgO contents in the reconstructed whole rock for this study. The size of most xenoliths was 4 cm × 6 cm × 4 cm (Fig. 2a). Eclogite and pyroxenite xenoliths from Obnazhennaya have previously been investigated for major, trace elements, oxygen isotope, and Sr–Nd isotopes by Qi et al. (1994); Taylor et al. (2003); Alifirova et al. (2012, 2015) and Spengler and Alifirova (2019). In these studies, nearly all of samples were of group A (or high-MgO eclogites and websterites). Only three samples from Taylor et al. (2003) are Group B eclogites with low MgO contents and without orthopyroxene and are, thus, similar to the samples in this study. No detailed petrographic descriptions for these three samples were reported, but their mineral major and trace-element compositions and garnet oxygen isotopes exist; these data are included and discussed in this study.

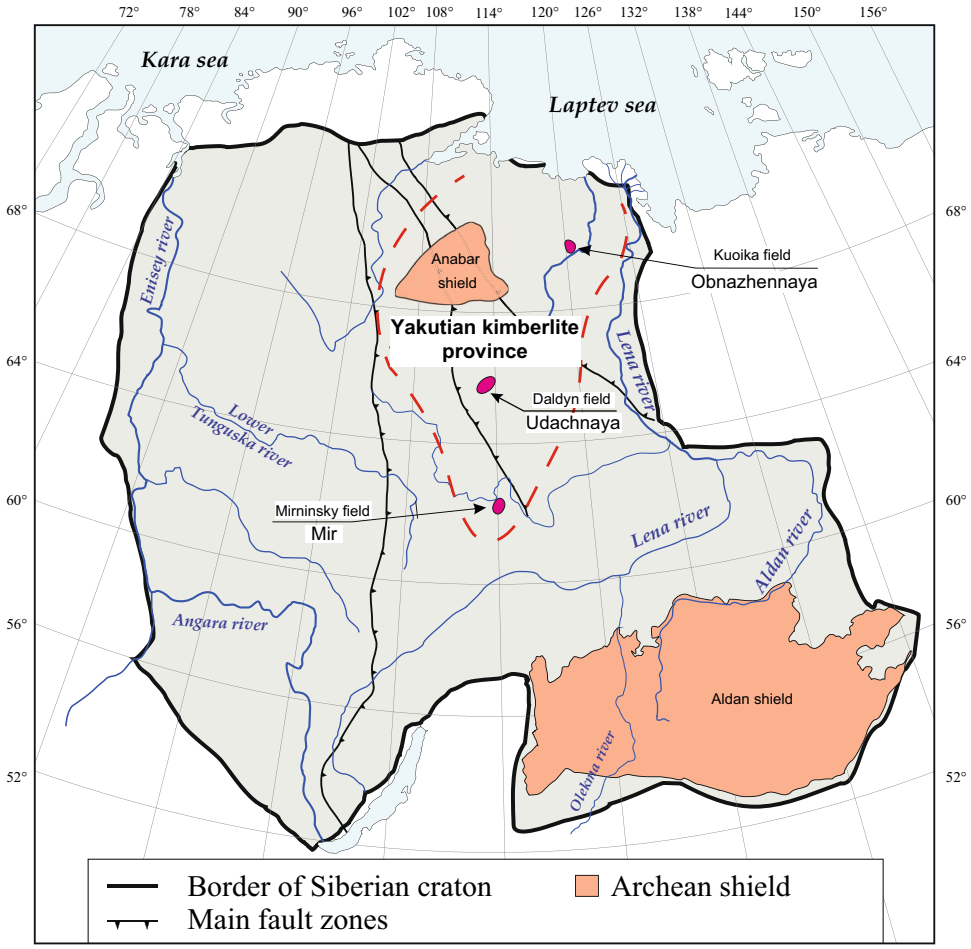

Fig. 1 Simplified geological map of the Siberian platform, which is modified. The Obnazhennaya kimberlite pipe, host of the eclogite xenoliths in this study, is located at the north-eastern margin of the platform. The Udachnaya kimberlite pipe from the Daldyn filed and Mir kimberlite from Mirninsky field are located in the central part of the platform [Modified from Griffin et al. (1999)]

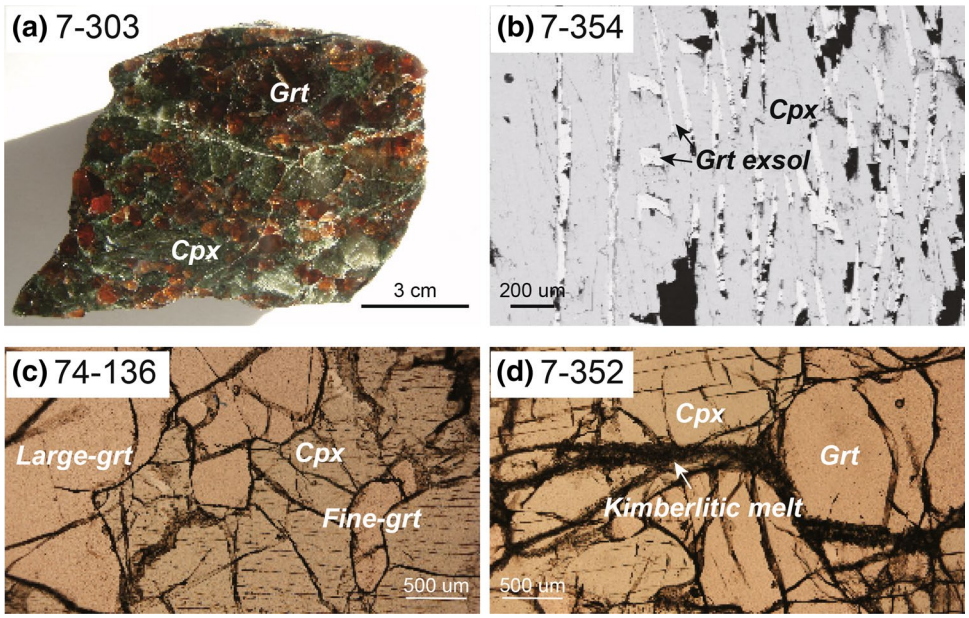

Fig. 2 Typical textures in the Obnazhennaya eclogite suite. **a** Equigranular texture of garnet and clinopyroxene, sample 7-303; **b** garnet exsolution lamellae in clinopyroxene, sample 7-354; **c** coarse and fine garnets, sample 74-136; **d** a complex network of fractures filled with kimberlitic melt, sample 7-352. *Grt* garnet, *Cpx* clinopyroxene

Analytical methods

Modal mineralogy

Modal abundances were obtained by point counting of thin sections. The points were spaced 0.5 mm apart and between 200 and 600 points were counted, depending on the size of the thin section as well as the mineral size. Coarse-grained garnet, fine-grained garnet, garnet exsolution lamellae in clinopyroxene and clinopyroxene were distinguished in the point counting. Melt veins (described below) were omitted when calculating the modal mineralogy.

Major and trace elements

Major-element compositions of minerals were analyzed with a JEOL JXA-8100 Electron Probe at the National Astronomical Observatories, Chinese Academic of Sciences, using a 15 keV accelerating voltage and a 10 nA beam current. Multiple grains of garnet and clinopyroxene were analyzed from each xenolith, with a minimum of five analyses per mineral grain. A variety of natural and synthetic standards were used to calibrate the major components, some of which were also measured as unknowns to monitor data quality (see Appendix 1). The ZAF model (Armstrong 1995) was applied for matrix correction. The two-sigma analytical precision of most elements (Si, Al, Ca, Fe, Mg, Na, Mn) analyzed by EPMA is ca. 2%.

Trace elements in clinopyroxenes and different types of garnets were analyzed using laser ablation inductively coupled plasma mass spectrometer (LA-ICP-MS) at China University of Geosciences, Beijing. The LA-ICP-MS system consists of a 193 nm pulsed ArF excimer laser coupled to an Agilent 7500 quadrupole ICP-MS. Isotopes were measured in peak-hopping mode. A spot size of 80 µm and a repetition rate of 8 Hz were used. The NIST 612 glass was used as an external calibration standard and the isotope ^{43}Ca was used as an internal standard. BHOV-2 glass was measured as an unknown to verify data accuracy, and their results are illustrated in Appendix 1. The analytical precision of most elements analyzed by the LA-ICP-MS method is ca. 5–10%.

Oxygen isotopes by SIMS

Oxygen-isotope compositions of garnet were analyzed in situ using a CAMECA SIMS 1280 ion microprobe at the University of Wisconsin-Madison. Samples were lightly crushed and clean garnets (1–3 mm) were handpicked with a binocular microscope. Separated garnet grains were mounted within 7.5 mm of the center of an epoxy disk with the UWG-2 garnet standard at the center of the mount, and then polished to a flat, smooth surface. The $^{133}Cs^{+}$ primary ion beam (20 kV total accelerating voltage) was focused to a diameter of ~ 10 µm on the gold-coated sample surface. Secondary O^{-} ions were accelerated away from the sample by ~ 10 kV and the analysis site was centered under a uniform electron field generated by a normal-incidence electron gun for charging compensation. Due to the different compositions between garnet standard UWG-2 and the Obnazhennaya garnets, a matrix effect is present. To account for the matrix effects, 16 in-house garnet standards from five garnet end members (pyrope, almandine, spessartine, grossular and andradite) were analyzed to calculate the working curve line and instrument bias relative to UWG-2 one day before running the unknowns. The Obnazhennaya garnets were then plotted on the working curve line based on their compositions, and the bias of each unknown relative to UWG-2 was calculated. Details are provided in Page et al. (2010) and Kitajima et al. (2016), and we provide only a short summary here. Four points on UWG-2 were analyzed before and after every 10–15 unknown sample points. The $\delta^{18}O_{VSMOW}$ value of UWG-2 standard is + 5.8‰ (Valley et al. 1995). Point-to point precision for $\delta^{18}O$ was typically better than 0.4‰ (2 SD).

Results

Petrography

The low-MgO Obnazhennaya eclogites are bimineralic, with light to dark green clinopyroxene and orange to pale pink garnets. Accessory sulfides occur in most samples, whereas rutile, ilmenite and orthopyroxene were not observed. The modal mineralogy varies considerably, with garnet proportions of 27–76 vol% and clinopyroxene of 24–73 vol%. Complete petrographic descriptions are provided in Appendix 2.

The eclogites commonly have a planar fabric defined by subhedral to elongated garnets within a matrix of coarse and interlocking clinopyroxenes. Some eclogites have poikilitic microstructures with garnet enclosing clinopyroxene. All textural types of clinopyroxene typically contain needle and/or lamellae-shaped elongate garnets with a shape-preferred orientation (Fig. 2b), up to 0.7 mm across. By contrast, granular garnets contain no exsolution lamellae, and can be subdivided into two types based on their grain sizes: coarse and fine. The coarse-grained garnets (2–10 mm; Fig. 2c) represent 80 vol% of total garnets and have smooth rims, whereas fine-grained garnets (0.05–2 mm; Fig. 2c) have euhedral-to-subhedral texture and are embedded in clinopyroxenes.

All samples are fresh, as alteration products account for < 1 vol% of these samples, although fractures containing kimberlitic melt (Fig. 2d) cross-cut the samples and some

Table 1 Major element compositions (wt%) of minerals from the Obnazhennaya eclogites

Sample	Mineral	Modal	SiO_2	TiO_2	Al_2O_3	Cr_2O_3	FeO	MnO	MgO	CaO	Na_2O	K_2O	NiO	Total	Mg#	Jd
Obn7-303	Cpx	0.485	53.76	0.11	6.32	0.05	2.96	0.01	13.16	19.62	2.93	0.01	0.05	98.99	88.88	0.21
	Grt-coarse	0.439	40.43	0.04	22.73	0.05	13.53	0.38	13.33	8.80	0.02	0.01	0.01	99.33	63.94	
	Grt-fine	0.032	40.10	0.02	22.58	0.03	13.26	0.38	11.96	10.82	0.01	0.00	0.01	99.17	61.87	
	Grt-lamella	0.044	40.00	0.01	22.21	0.06	12.57	0.34	10.30	13.37	0.01	0.00	0.01	98.87	59.61	
Obn7-350	Cpx	0.451	53.30	0.14	6.17	0.04	2.61	0.04	13.44	17.62	3.25	0.01	0.12	96.72	90.27	0.25
	Grt-coarse	0.529	40.91	0.04	23.07	0.04	11.33	0.20	18.21	4.41	0.01	0.01	0.02	98.25	74.32	
	Grt-fine	0.006	40.64	0.06	22.95	0.03	11.41	0.21	18.08	4.19	0.01	0.01	0.01	97.59	74.04	
	Grt-lamella	0.014	40.45	0.03	22.81	0.05	11.44	0.22	17.91	3.53	0.01	0.00	0.02	96.48	73.81	
Obn7-352	Cpx	0.498	53.38	0.12	8.27	0.10	2.70	0.01	12.29	18.66	3.30	0.00	0.07	98.91	89.12	0.24
	Grt-coarse	0.488	41.05	0.03	22.91	0.08	12.79	0.31	14.61	8.12	0.01	0.01	0.01	99.92	67.27	
	Grt-fine	0.014	40.71	0.04	22.60	0.09	12.32	0.30	13.19	9.81	0.01	0.01	0.01	99.07	65.84	
Obn7-354	Cpx	0.727	53.14	0.08	6.98	0.05	2.93	0.02	12.73	19.14	3.02	0.01	0.07	98.18	88.65	0.22
	Grt-coarse	0.229	40.57	0.01	22.74	0.03	13.84	0.39	13.06	8.85	0.02	0.01	0.02	99.54	62.95	
	Grt-fine	0.011	40.15	0.02	22.50	0.03	12.48	0.32	10.48	12.70	0.01	0.00	0.02	98.71	60.18	
	Grt-lamella	0.033	39.76	0.04	22.08	0.03	11.97	0.28	8.96	15.45	0.01	0.01	0.01	98.60	57.40	
Obn7-379	Cpx	0.241	53.30	0.18	6.46	0.08	3.03	0.02	13.02	19.12	3.03	0.00	0.06	98.30	88.55	0.22
	Grt-coarse	0.728	40.45	0.05	22.66	0.08	13.31	0.37	13.96	8.25	0.02	0.01	0.02	99.15	65.38	
	Grt-fine	0.011	40.55	0.03	22.63	0.06	13.18	0.35	13.00	9.68	0.01	0.01	0.00	99.51	63.96	
	Grt-lamella	0.020	39.92	0.02	22.45	0.07	12.99	0.35	11.94	10.64	0.02	0.01	0.01	98.41	62.33	
Obn7-394	Cpx	0.569	51.53	0.05	15.39	0.05	1.12	0.00	8.90	17.66	4.44	0.01	0.13	99.28	93.46	0.31
	Grt-coarse	0.390	41.33	0.01	23.39	0.28	8.04	0.17	16.55	9.04	0.01	0.01	0.02	98.85	78.74	
	Grt-fine	0.014	41.33	0.00	23.58	0.05	7.28	0.16	13.85	13.32	0.01	0.00	0.01	99.59	77.41	
	Grt-lamella	0.027	41.81	0.03	23.63	0.07	5.49	0.09	9.37	21.13	0.02	0.00	0.00	101.64	75.45	
Obn74-136	Cpx	0.617	53.17	0.09	6.20	0.04	3.54	0.02	13.02	19.70	2.67	0.00	0.04	98.49	86.88	0.20
	Grt-coarse	0.330	40.05	0.02	22.45	0.03	15.15	0.40	12.44	8.35	0.00	0.00	0.00	98.91	59.64	
	Grt-lamella	0.053	39.80	0.03	22.32	0.04	14.22	0.32	9.18	13.61	0.01	0.00	0.01	99.53	53.75	
Obn74-639	Cpx	0.488	53.76	0.04	6.15	0.01	3.21	0.03	13.39	19.85	2.67	0.01	0.05	99.17	88.26	0.20
	Grt-coarse	0.472	40.15	0.02	22.56	0.01	14.03	0.43	12.60	9.32	0.02	0.01	0.02	99.17	61.79	
	Grt-fine	0.024	40.15	0.02	22.55	0.01	13.65	0.41	11.81	10.45	0.02	0.00	0.03	99.10	60.89	
	Grt-lamella	0.016	39.68	0.02	22.22	0.01	13.28	0.37	10.30	12.77	0.02	0.00	0.00	98.66	58.27	

cpx clinopyroxene, *grt* garnet, *grt-coarse* garnet coarse garin with size larger than 2 mm, *grt-fine* garnet fine grain with size ranging from 0.05 to 2 mm, *grt-lamella* garnet lamellae in clinopyroxene, *Jd* Jadite

mineral grains. Moreover, neither serpentine nor phlogopite was observed in any samples.

Mineral major elements

Clinopyroxenes are homogeneous within the analytical uncertainty (Table 1). All eight samples have jadeite (Na/Na+Ca) component in clinopyroxene > 0.2, indicating that all low-MgO samples are true eclogites (Clark et al. 1968), rather than garnet clinopyroxenites. Compared with the Obnazhennaya Group B eclogites previously studied (Taylor et al. 2003), clinopyroxenes in our samples have lower FeO contents (1.1–3.5 wt% vs. 4.3–5.1 wt%) and higher Mg# (Mg# = 100*Mg/(Mg+Fe); 86.9–93.5 vs. 79.5–83.8). In addition, the clinopyroxenes in this study are slightly less jadeite-rich (0.20–0.31) compared to those of the previous study (0.29–0.35; Taylor et al. 2003). Clinopyroxene in sample 7-394 contains the highest Al_2O_3 (15.4 wt%) and Mg# (93.5), and the lowest MgO (8.90 wt%) and FeO (1.12 wt%) compared with the rest of the samples.

Garnets of different textural types are compositionally distinct, with the exception of those in sample 7-350. Compared to the coarse-grained garnets, fine-grained and lamellar garnets in clinopyroxene have higher CaO (9.7–21.1 wt% vs. 8.1–9.3 wt%) and lower MgO (9.0–13.9 wt% vs. 12.4–16.6 wt%). Lamellar garnets in each sample have the highest CaO (10.6–21.1 wt%) and lowest MgO (9.0–11.9 wt%) (Table 1; Appendix 3). Among these, garnet in sample 7-394 has the lowest FeO (5.5–8.0 wt%) and highest Mg# (75.4–78.7) of all garnet types. By contrast, garnets of different sizes are homogeneous in sample 7-350, and they have the highest

Table 2 Trace-element composition of garnets, clinopyroxenes from Obnazhennaya eclogites in ppm

	7-303-cpx	7-303-grt-coarse	7-303-grt-fine	7-352-cpx	7-352-grt-coarse	7-352-grt-fine	7-354-cpx	7-354-grt-coarse	7-354-grt-fine	7-379-cpx	7-379-grt-coarse	7-379-grt-fine
Vol	0.529	0.439	0.032	0.498	0.488	0.014	0.727	0.262	0.011	0.261	0.728	0.011
V	782	299	188	435	176	137	785	227	256	849	289	243
Cr	319	287	151	626	683	569	192	188	200	427	451	434
Th	0.070	0.001	0.001	0.011	0.001	0.001	0.070	0.002	0.002	0.049	0.001	0.17
U	0.049	0.002	0.002	0.008	0.001	0.001	0.054	0.004	0.004	0.035	0.002	0.004
Nb	0.66	0.010	0.009	0.020	0.003	0.002	0.82	0.025	0.031	0.35	0.011	0.015
Ta	0.015	0.001	0.001	0.001	0.001	0.011	0.026	0.001	0.001	0.009	0.001	0.001
La	0.653	0.005	0.002	0.084	bdl	0.002	1.08	0.003	0.003	0.61	0.004	0.005
Ce	1.21	0.009	0.007	0.14	0.002	0.003	2.15	0.013	0.019	1.05	0.008	0.011
Pr	0.11	0.004	0.004	0.026	0.003	0.001	0.22	0.005	0.006	0.11	0.005	0.006
Sr	29.5	0.025	0.07	9.78	0.014	0.011	40.2	0.020	0.028	30.5	0.020	0.037
Nd	0.49	0.050	0.05	0.25	0.070	0.065	0.78	0.066	0.11	0.57	0.077	0.082
Sm	0.10	0.14	0.09	0.19	0.23	0.18	0.078	0.095	0.14	0.13	0.15	0.15
Zr	0.61	0.57	0.30	0.87	1.23	0.50	0.61	0.29	0.32	1.70	1.08	0.79
Hf	0.033	0.023	0.01	0.054	0.051	0.018	0.029	0.008	0.010	0.11	0.030	0.012
Eu	0.040	0.14	0.09	0.080	0.25	0.20	0.041	0.092	0.13	0.079	0.16	0.15
Ti	662	272	157	948	393	252	513	170	210	875	317	254
Gd	0.072	0.67	0.35	0.15	1.04	0.74	0.077	0.433	0.47	0.17	0.73	0.62
Tb	0.008	0.21	0.14	0.018	0.29	0.19	0.006	0.154	0.12	0.021	0.23	0.19
Dy	0.021	2.29	1.10	0.079	2.48	1.33	0.033	1.59	1.01	0.10	2.32	1.76
Y	0.061	17.8	8.41	0.19	15.1	7.58	0.088	12.3	5.63	0.36	17.5	12.8
Ho	0.003	0.67	0.31	0.007	0.62	0.30	0.003	0.45	0.22	0.015	0.64	0.48
Er	0.005	2.14	0.97	0.018	1.81	0.77	0.006	1.53	0.55	0.030	2.18	1.58
Tm	0.001	0.36	0.15	0.002	0.26	0.11	0.002	0.25	0.070	0.003	0.34	0.24
Yb	0.003	2.62	1.07	0.007	2.03	0.70	0.004	1.90	0.36	0.015	2.77	1.69
Lu	0.001	0.41	0.15	0.001	0.27	0.10	0.001	0.30	0.046	0.002	0.41	0.28

Element	7-394-cpx	7-394-grt-coarse	7-394-grt-fine	74-136-cpx	74-136-grt-coarse	74-136-grt-lamellae	74-639-cpx	74-639-grt-coarse	74-639-grt-fine	7-350-cpx	7-350-grt-coarse
Vol	0.596	0.390	0.014	0.617	0.330	0.053	0.504	0.472	0.024	0.465	0.535
V	183	51.0	55.0	509	197	143	779	271	209	148	37.6
Cr	407	255	299	247	231	198	35.6	38.8	25.8	262	289
Th	0.002	0.004	0.001	0.005	bdl	0.001	0.003	0.001	bdl	0.024	0.004
U	0.004	0.11	0.001	0.003	bdl	0.002	0.001	0.001	bdl	0.007	0.003
Nb	0.014	0.042	0.006	0.010	0.003	0.007	0.007	0.002	bdl	0.036	0.005
Ta	0.001	0.001	0.001	0.000	bdl	0.0005	0.001	0.001	0.001	0.004	0.001
La	0.004	0.003	0.024	0.052	0.002	0.002	0.15	bdl	0.005	0.75	0.033

Table 2 (continued)

Element	7-394-cpx	7-394-grt-coarse	7-394-grt-fine	74-136-cpx	74-136-grt-coarse	74-136-grt-lamellae	74-639-cpx	74-639-grt-coarse	74-639-grt-fine	7-350-cpx	7-350-grt-coarse
Ce	0.032	0.005	0.006	0.069	0.002	0.002	0.48	0.011	0.009	1.82	0.030
Pr	0.021	0.004	0.010	0.008	0.003	0.001	0.070	0.008	0.004	0.27	0.008
Sr	11.1	0.061	0.065	3.60	bdl	0.013	22.3	0.032	0.025	168	0.047
Nd	0.21	0.074	0.165	0.043	0.011	0.016	0.27	0.045	0.035	1.56	0.077
Sm	0.068	0.17	0.19	0.051	0.046	0.052	0.040	0.056	0.061	0.57	0.16
Zr	0.20	0.82	0.50	0.13	0.075	0.042	0.22	0.14	0.13	7.32	2.61
Hf	0.015	0.032	0.020	0.014	0.006	0.003	0.018	0.012	0.003	0.24	0.040
Eu	0.027	0.21	0.22	0.036	0.085	0.077	0.028	0.092	0.073	0.31	0.23
Ti	364	107	106	510	197	141	353	172	112	761	278
Gd	0.023	0.41	0.38	0.088	0.42	0.33	0.070	0.47	0.35	0.40	0.58
Tb	0.003	0.11	0.073	0.011	0.13	0.079	0.012	0.18	0.12	0.040	0.13
Dy	0.014	0.83	0.46	0.056	1.12	0.62	0.046	1.73	1.00	0.13	0.91
Y	0.017	5.30	2.34	0.16	7.88	3.67	0.16	13.4	6.63	0.36	4.71
Ho	0.002	0.21	0.091	0.007	0.29	0.15	0.007	0.52	0.24	0.016	0.20
Er	0.003	0.66	0.24	0.011	0.87	0.34	0.014	1.65	0.67	0.025	0.50
Tm	0.002	0.11	0.036	0.002	0.13	0.043	0.001	0.26	0.085	0.003	0.063
Yb	0.006	0.82	0.25	0.008	0.90	0.23	0.004	1.91	0.55	0.018	0.47
Lu	0.002	0.13	0.033	0.002	0.13	0.030	0.001	0.28	0.073	0.001	0.078

bdl below detection limit

MgO (17.9–18.2 wt%), but the lowest CaO (3.5–4.4 wt%) contents.

Trace elements

The trace-element compositions of minerals from Obnazhennaya eclogites are given in Table 2 and presented as chondrite-normalized (McDonough and Sun 1995) REE (rare earth element) plots in Fig. 3, along with previously published data (Taylor et al. 2003).

Clinopyroxenes exhibit variable REE concentrations and patterns. All are convex-upwards, but some are LREE-enriched, while others are LREE-depleted, and all exhibit positive Eu anomalies relative to their neighboring REE with Eu/Eu* (chondrite-normalized Eu/$(Sm \times Gd)^{0.5}$) ranging from 1.4 to 2.4 (Fig. 3a). The REE patterns of clinopyroxenes in this study overlap with those in the previous study, but ours have overall lower REE concentrations and higher Eu/Eu*.

Coarse-grained garnets show typical LREE-depleted chondrite-normalized REE patterns (Fig. 3b), with La_N of 0.1–2.3 and Yb_N of 1.6–9.8. These samples have similar HREE contents as garnets in the previous study (Taylor et al. 2003), but our samples have lower LREE contents. Coarse-grained garnets from both this and the previous study show variable, positive Eu anomalies (Fig. 3b), with Eu/Eu* of 1.4–2.4. Fine-grained garnets from six samples were analyzed, but garnet lamellae in clinopyroxene could only be analyzed in one sample due to the typically small sizes. The fine-grained and lamellar garnet have similar REE patterns to each other, with overall lower HREE contents and negative sloped HREE patterns compared to the coarse-grained garnets (Fig. 3b).

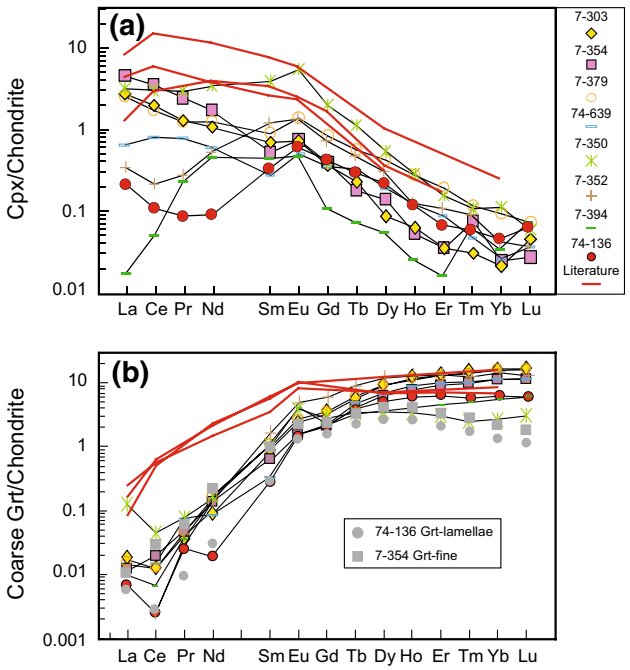

Fig. 3 **a** Chondrite-normalized REE patterns of clinopyroxenes from the Obnazhennaya low-MgO eclogites; **b** chondrite-normalized REE patterns of coarse garnets from the Obnazhennaya low-MgO eclogites. Grey cycles and squares are REE patterns of garnet lamellae in clinopyroxene from 74-136 and fine garnet from 7-354. Red lines in both **a** and **b** are Obnazhennaya Group B eclogites from Taylor et al. (2003). Chondrite values from McDonough and Sun (1995)

Reconstructed whole-rock compositions

Bulk rock chemical analyses of kimberlite-hosted xenolithic eclogites have been shown to represent mixtures of the original eclogite and host kimberlite (e.g., Barth et al. 2001; Jacob et al. 2005). We, therefore, calculated bulk rock compositions for major and trace elements from garnet and clinopyroxene using modal abundances (determined by point counting) and the results are listed in Tables 3 and 4, respectively. Garnets of all textural types are all accounted for in such calculations for both major and trace elements. Modal abundances of garnet lamellae in clinopyroxenes for some samples were considered part of the clinopyroxene mode while calculating their trace elements. Whole-rock reconstruction is not particularly sensitive to variations in modes as the calculated whole-rock trace-element patterns do not change significantly when the garnet (grt): clinopyroxene (cpx) ratios vary between 50:50 and 70:30 (Jacob and Foley 1999).

Table 3 Estimated major element compositions (wt%) of reconstructed bulk rocks of Obnazhennaya eclogites

Sample	SiO_2	TiO_2	Al_2O_3	Cr_2O_3	FeO	MnO	MgO	CaO	Na_2O	K_2O	NiO	Total	Mg#
7-303	46.86	0.07	14.74	0.05	8.36	0.20	13.07	14.31	1.43	0.01	0.03	99.14	73.8
7-350	46.49	0.08	15.45	0.04	7.40	0.13	16.05	10.36	1.47	0.01	0.06	97.53	79.6
7-352	47.18	0.07	15.61	0.09	7.76	0.16	13.43	13.39	1.65	0.00	0.04	99.40	75.7
7-354	49.68	0.06	11.26	0.04	5.84	0.12	12.66	16.59	2.20	0.01	0.06	98.51	79.6
7-379	43.53	0.08	18.76	0.08	10.82	0.28	13.68	10.93	0.74	0.01	0.03	98.93	69.5
7-394	47.15	0.03	18.85	0.14	4.02	0.07	11.97	14.33	2.53	0.01	0.08	99.18	84.3
74-136	48.13	0.06	12.41	0.04	7.94	0.16	12.62	15.63	1.65	0.00	0.03	98.68	74.1
74-639	46.78	0.03	14.54	0.01	8.73	0.24	12.93	14.54	1.31	0.01	0.03	99.16	72.7

Table 4 Estimated trace-element compositions (ppm) of reconstructed bulk rocks of Obnazhennaya eclogites

Sample	7-303	7-350	7-352	7-354	7-379	7-394	74-136	74-639
V	545	88.9	304	633	434	130	389	526
Ni	240	478	311	443	208	641	220	271
Cr	295	277	653	191	445	346	241	36.9
Th	0.038	0.013	0.006	0.052	0.015	0.003	0.003	0.002
U	0.027	0.005	0.004	0.040	0.010	0.045	0.002	0.001
Nb	0.35	0.019	0.011	0.60	0.10	0.025	0.007	0.005
Ta	0.008	0.002	0.001	0.019	0.003	0.001	0.0003	0.001
La	0.35	0.37	0.042	0.78	0.16	0.004	0.033	0.078
Ce	0.64	0.86	0.068	1.57	0.28	0.021	0.043	0.25
Pr	0.062	0.13	0.014	0.16	0.033	0.014	0.006	0.039
Sr	15.6	78.3	4.87	29.2	7.97	6.63	2.22	11.3
Nd	0.28	0.76	0.16	0.59	0.20	0.16	0.031	0.16
Sm	0.12	0.35	0.21	0.083	0.15	0.11	0.050	0.048
Zr	0.57	4.80	1.04	0.53	1.24	0.44	0.11	0.18
Hf	0.027	0.13	0.052	0.024	0.050	0.022	0.011	0.015
Eu	0.083	0.27	0.16	0.056	0.14	0.10	0.055	0.059
Ti	470	502	667	419	462	260	389	262
Gd	0.33	0.50	0.59	0.17	0.58	0.18	0.21	0.26
Tb	0.10	0.088	0.15	0.046	0.18	0.045	0.056	0.094
Dy	1.02	0.54	1.27	0.45	1.74	0.34	0.45	0.87
Y	7.83	2.69	7.56	3.35	13.0	2.11	2.97	6.56
Ho	0.30	0.12	0.31	0.12	0.48	0.084	0.11	0.26
Er	0.94	0.28	0.90	0.41	1.61	0.26	0.32	0.80
Tm	0.16	0.035	0.13	0.068	0.25	0.044	0.046	0.12
Yb	1.15	0.26	1.01	0.50	2.04	0.33	0.32	0.92
Lu	0.18	0.042	0.13	0.079	0.30	0.052	0.047	0.14

Reconstructed bulk major element compositions of the Obnazhennaya low-MgO eclogites have Mg-numbers ranging from 69.5 to 84.3, overlapping, but ranging to higher values than the three Group B samples from the previous study (60.8–74.4). Bulk CaO concentrations are high, from 10.9 to 16.6 wt%. Sample 7-394 has the highest Al_2O_3 (18.9 wt%) and Na_2O (2.5 wt%) contents and the highest Mg# (84.3). Sample 7-350 has the highest MgO (16.1 wt%) content, whereas most others have MgO contents ranging from 12.0 to 13.7 wt%.

All Obnazhennaya low-MgO eclogites except 7-350 have flat to positively sloped HREEs (heavy rare earth elements), MREE (medium rare earth elements)-depleted REE patterns ($(Nd/Yb)_N = 0.03–0.46$) and positive Eu anomalies (Fig. 4a). Most of the samples are LREE-enriched, whereas others have flat to depleted LREE patterns. All samples are also enriched in Sr (positive Sr anomaly) relative to elements of similar incompatibility in basaltic systems (Fig. 4b). Sample 7-350, with the largest Eu and Sr anomaly, has a flat REE pattern with $(Nd/Yb)_N = 1.0$. The MREE and HREE abundances of the eclogites are both lower and higher than those of the primitive mantle (Fig. 4b). Three Group B samples from the previous study show similar HREE contents, but higher LREE concentrations compared to samples in this study (Qi et al. 1994; Taylor et al. 2003). Rutile dominates the budget of TiO_2, Nb, Ta, Zr and Hf in eclogites (Rudnick et al. 2000) and negative anomalies for these elements in the reconstructed bulk rocks suggest that rutile may exist in Obnazhennaya low-MgO eclogites, but was not present in the thin sections we studied. Because of these uncertainties, the calculated TiO_2, Nb and Ta in the reconstructed bulk rocks will not be used in further discussion.

Oxygen isotopes

In eclogite xenoliths, garnet is considered to preserve oxygen isotopic ratios more reliably than clinopyroxene for two reasons (1) oxygen diffuses more slowly in garnet than clinopyroxene at mantle temperatures (Farver 2010; Zhang et al. 2016) and (2) garnet is more resistant to overprinting processes than clinopyroxene (Deines and Haggerty 2000). Deines et al. (1991) found that the $\Delta^{18}O$ between garnet and clinopyroxene varies with temperature. Samples with equilibrium temperature of 800–1000 °C have 0.6–0.4‰ $\Delta^{18}O_{grt-cpx}$ (Fig. 8 in Radu et al. 2019), and the resultant difference between garnet and whole rock is less than 0.5‰

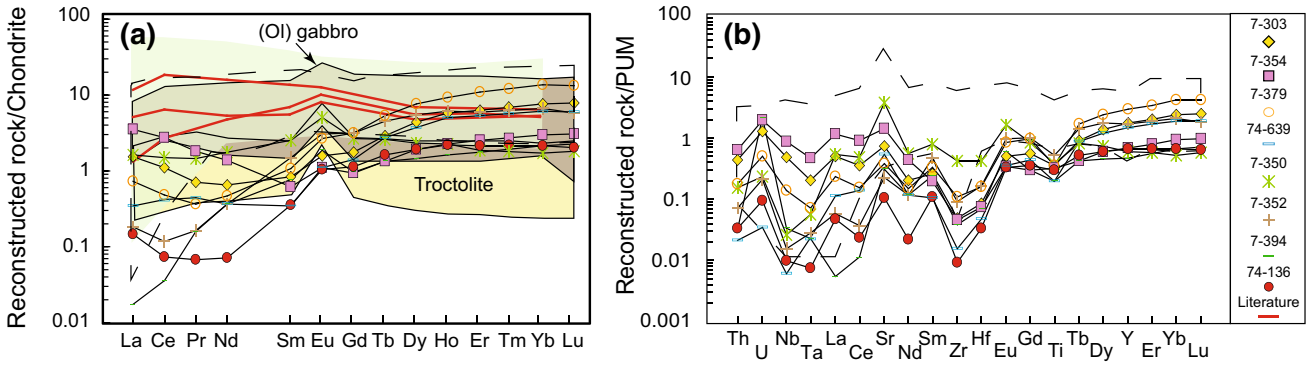

Fig. 4 **a** Chondrite-normalized reconstructed bulk REE concentrations of low-MgO eclogites estimated from the REE concentrations in minerals and their modes from Table 2. The compositional field of olivine gabbros from the MARK region, mid-Atlantic ridge is shown as the brown field (Casey 1997) and the range of troctolite compositions from IODP Site U1309 in Mid-Atlantic Ridge (Godard et al. 2009) and the Pito Deep in the Pacific (Perk et al. 2007) is shown as a yellow field. Dashed line field and light green field mark the composition of Udachnaya low-MgO eclogites and Mir low-MgO eclogite xenoliths, respectively. Data of low-MgO eclogites from Udachnaya and Mir kimberlite is from Agashev et al. (2018) and Beard et al. (1996), respectively. Red lines are Obnazhennaya Group B eclogites from Taylor et al. (2003). Data are normalized to chondrite values from McDonough and Sun (1995). **b** Primitive mantle-normalized reconstructed whole-rock trace-element diagram for Obnazhennaya low-MgO eclogites. Data are normalized to the primitive mantle of McDonough and Sun (1995). Dash line field represents the Udachnaya low-MgO eclogite xenoliths (Agashev et al. 2018)

(based on the function: $\delta^{18}O_{\text{whole rock}} = \delta^{18}O_{\text{grt}}$*grt vol% + ($\delta^{18}O_{\text{grt}} - \Delta^{18}O_{\text{grt-cpx}}$)*cpx vol%). Therefore, the $\delta^{18}O$ value in garnet approximates the $\delta^{18}O$ value of the bulk rock (Korolev et al. 2018). Hence, garnet oxygen analyses are generally used to represent eclogite whole-rock oxygen isotopic compositions.

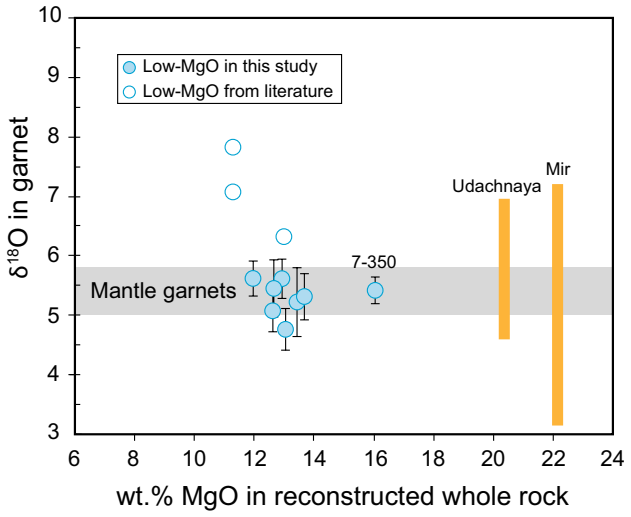

Fig. 5 MgO in reconstructed whole-rock vs. $\delta^{18}O$ in garnet for Obnazhennaya low-MgO eclogites. The grey filed depicts the range of mantle garnets that shifts towards lighter isotopic composition by 0.1‰ relative to the whole-rock mantle range due to the fractionation between garnet and whole rock at 1000–1200 °C (Deines et al. 1991). Vertical error bars are two sigma uncertainties for the oxygen isotopes. Open circles are Obnazhennaya Group B eclogites from Taylor et al. (2003). $\delta^{18}O$ in garnet for Udachnaya low-MgO eclogites are from Jacob et al. (1994) and Shatsky et al. (2016) and data for Mir low-MgO eclogites are from Beard et al. (1996)

Both coarse- and fine-grained garnets were analyzed, and in all cases, the oxygen-isotope compositions of different sized garnets are identical, within error. Garnets in this study have a restricted range of $\delta^{18}O$ values (4.73–5.62‰; Table 5), most of which lie within the mantle range ($\delta^{18}O = 5.5 \pm 0.4$‰; Mattey et al. 1994; Fig. 5). However, the three Group B eclogites from the previous study have heavier garnet $\delta^{18}O$ values ranging from 6.3 to 7.8‰ (Taylor et al. 2003).

Geothermobarometry

Temperatures were calculated using the garnet–clinopyroxene Fe^{2+}-Mg^{2+} exchange thermometer of Krogh (1988) and Krogh (2000) and pressures were calculated with the garnet–clinopyroxene geobarometer of Beyer et al. (2015). The Beyer et al. (2015) barometer formulation should only be applied to clinopyroxenes with low jadeite component and Si cations per formula unit below 1.985, as it is the case for all Obnazhennaya low-MgO eclogites. We applied these thermobarometers to the average EPMA analyses for clinopyroxenes and the garnet lamellae in clinopyroxenes, which should record the last stage of equilibration in the mantle. Fe^{3+} in garnet and clinopyroxene should be low to very low, as reflected by the sum of cations. Furthermore, Purwin et al. (2013) found, from high pressure experiments, that the partitioning of Fe^{3+} between the two phases is such that calculated temperatures are not significantly different

Table 5 Oxygen-isotope composition (δ18OVSMOW‰) of garnets from Obnazhennaya eclogites

Sample	$\delta^{18}O_{VSMOW}$‰	2SD
7-303	4.73	0.37
7-352	5.22	0.58
74-639	5.61	0.33
7-379	5.31	0.39
7-354	5.45	0.48
7-394	5.62	0.29
74-136	5.07	0.35
7-350	5.42	0.22

$\delta^{18}O_{VSMOW}‰ = [(^{18}O/^{16}O_{sample} - {}^{18}O/{}^{16}O_{SMOW})/{}^{18}O/{}^{16}O_{SMOW}]*1000$

SMOW standard mean ocean water

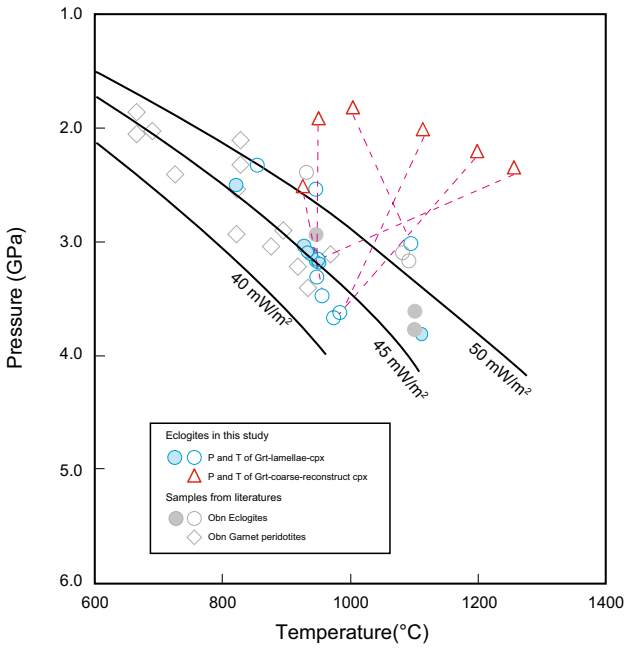

Fig. 6 Pressures and temperatures of the last equilibration of Obnazhennaya xenolithic low-MgO eclogites. Blue circles and red triangles represent Obnazhennaya eclogites in this study. Temperatures and pressures of blue circles are calculated from garnet-lamellae/garnet-fine (7-352)—host clinopyroxene, and the red triangles are calculated from garnet-coarse—reconstruct clinopyroxene. Grey circles are Obnazhennaya Group B eclogites calculated using the data from Taylor et al. (2003). Temperatures were calculated using the cpx–grt Fe–Mg exchange thermometer of Krogh (1988). Open symbols represent that pressures calculated using the barometer of Beyer et al. (2015), which is based on the incorporation of tetrahedrally coordinated aluminum in cpx coexisting with garnet, whereas filled symbols represent that pressures based on applying the temperature to the 45 mW/m^2 geotherm. The temperatures and pressures of garnet-peridotites (grey diamonds) are from Howarth et al. (2014)

if either Fe^{total} is used or if Fe^{3+} in both garnet and clinopyroxene are considered. Therefore, Fe^{total} was used in the calculations.

The calculated equilibrium temperatures and pressures are given in Table 6 and plotted in Fig. 6. Pressures and temperatures of the three Group B eclogites from Taylor et al. (2003) were calculated here as well using the above thermobarometers. Pressures and temperatures of garnet peridotites from Obnazhennaya pipe (Howarth et al. 2014) are also plotted in Fig. 6. They scatter around a conductive geotherm of about 45 mW/m^2 (Chapman and Pollack 1977).

The temperatures and pressures of last equilibration, calculated from the garnet lamellae and their host clinopyroxenes range from 855 to 1095 °C and 2.3–3.7 GPa. The scatter for the eclogite PT conditions is much larger than for the garnet peridotites, which may be due to the larger uncertainty associated with the geothermobarometer combinations for eclogites relative to those for peridotites. Part of the eclogite PT conditions overlap with the geothermal gradient for peridotites, others are significantly higher. It appears that, overall, the Beyer et al. (2015) barometer tends to yield somewhat lower pressures and hence warmer geothermal gradient.

We further calculated PT conditions for the combination of reconstructed clinopyroxene (Table 7) + coarse-grained garnet, which may record the equilibrium conditions of the original eclogite-facies metamorphism. The results are also plotted in Fig. 6 (open red triangles) and connected by tie lines with their respective last equilibration, as recorded by the garnet lamellae PT conditions. The temperatures of the latter are lower by around 180 °C, on average, and the pressure is higher by ~ 1.5 GPa (Table 6).

Discussion

Pressure–temperature history

The two generations of garnets preserved within the eclogites provide insights into the PT history experienced by the samples. Equilibrium pressure–temperature estimates from the last stage of equilibrium (garnet lamellae—host cpx) place these eclogite xenoliths at moderate pressure–temperature conditions 2.3–3.7 GPa and 855–1095 °C in the upper mantle, scattered around the 45 mW/m^2 geotherm at the time of entrainment by the kimberlite. However, the combination of reconstructed initial clinopyroxene composition and garnet-coarse composition suggest that this suite of

Table 6 Results of pressure and temperatures of low-MgO Obnazhennaya eclogites

Sample	$T_{Cpx–Grt}$/°C Grt lamella–cpx	$T_{Cpx–Grt}$/°C Grt lamella–cpx	$P_{Cpx–Grt}$/GPa Grt lamella–cpx	$T_{Cpx–Grt}$/°C Grt coarse–reconstruct cpx	$P_{Cpx–Grt}$/GPa Grt coarse–reconstruct cpx
	Krogh (1988)	Krogh (2000)	Beyer et al. (2015)	Krogh (1988)	Beyer et al. (2015)
This study					
7-303	975	909	3.7	1198	2.2
7-350	855	840	2.3	1056	0.8
7-352	947	851	2.5		
7-354	984	927	3.6	1114	2.0
7-379	950	870	3.2	1288	2.3
7-394	1095	1041	3.0	1003	1.8
74-136	949	888	3.3	950	1.9
74-639	957	887	3.5	927	2.5
Previous study	Grt–cpx		Grt–cpx		
O-501	1083	1038	3.1		
O-927	933	884	2.4		
O-82-91	1093	1045	3.2		

xenoliths originally formed as higher temperatures eclogites 927–1288 °C, but at lower pressures (1.8–2.5 GPa; Fig. 6).

Garnet exsolution from clinopyroxene were previously described from Obnazhennaya by Jerde et al. (1993) from three corundum- and kyanite-bearing eclogites (only major elements) and in a conference abstract by Dobosi et al. (2007) from large clinopyroxene (3 cm; both major and trace elements). Similar exsolution features have also been found in xenolithic eclogites within kimberlite from other cratons (e.g., Beck 1907; Jerde et al. 1993), ultramafic rocks (Zhang and Liou 2003) and eclogites within serpentinites occurring in metamorphic complexes (e.g., Reiche and Bautsch 1985). It was suggested in previous studies that any process involving a pressure increase and/or temperature decrease may produce garnet exsolution lamellae in host clinopyroxenes (e.g., Zhang and Liou 2003; Harte and Gurney 1975), because the solubility of Ca-(and Mg-) Tschermaks (CaTs and MgTs) is exceeded. The solubility of CaTs in clinopyroxene increases with temperature and decreases with pressure (e.g., Gasparik 1984).

Reconstructed clinopyroxenes in our samples have CaTs ranging from 12 to 16 mol% for most samples except for two with 4 and 6 mol%. This is much higher than in the measured clinopyroxenes (Table 7). Such precursor phases of garnet + clinopyroxene intergrowth were considered to be primary high-aluminum pyroxene formed under higher temperature conditions (Zhang and Liou 2003). The calculated temperatures from the reconstructed clinopyroxene and coarse garnet are indeed higher and support a higher temperature origin. The granular garnets are precursor phases and did not participate in the reaction during exsolution. This is supported by the different REE patterns of coarse and lamellar garnets—the negative middle to heavy REE slopes of the lamellar garnets demonstrate equilibration with the host clinopyroxene but not with the granular garnets. Clinopyroxenes from experiments with a kyanite eclogite at 1100 °C and pressures between 2 and 3.5 GPa contain 15.7–19.3 wt% Al_2O_3 both as jadeite and CaTs components (Morishita et al. 2004), higher than our reconstructed precursor clinopyroxenes (6.7–15.8 wt%). The experimental results at similar pressures as the Obnazhennaya eclogites are a guide for the possible PT conditions for the formation of the precursor high Al-pyroxenes. The experimental clinopyroxenes are higher in Al_2O_3 because of the higher Na-content of the kyanite eclogite. The calculated PT conditions for the reconstructed cpx–granular grt pairs lie in the range of 2 GPa and 1000–1200 °C, far elevated above any continental conductive geothermal gradient, or modern subduction zone gradients. We explore, below, the implications of this PT history for the origin and devolution of the eclogites. First, though, we use their chemical characteristics to infer their origins.

Evaluation of the effects of metasomatism

Before the chemical composition of eclogites can be used to infer their origin, one must first evaluate whether they have experienced any metasomatism, which may affect xenolithic eclogites both during their residence in the cratonic lithosphere and/or during entrainment in the host kimberlite (Barth et al. 2001; Huang et al. 2012, 2014; Shu et al. 2018). Metasomatism can alter the chemical and isotopic compositions of a rock at different scales, cryptically to modally, obscuring the primary composition to varying

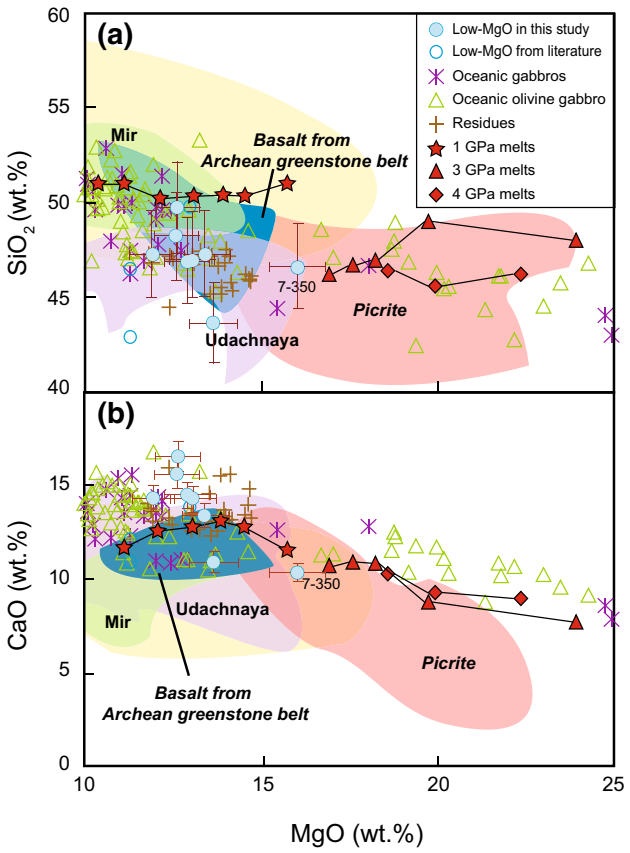

Fig. 7 Plot of MgO vs. SiO_2 (**a**) and CaO (**b**) for reconstructed Obnazhennaya eclogite whole-rock compositions. Blue circles: eclogites studied here. Blue open circles: Obnazhennaya Group B eclogites from Taylor et al. (2003). Pluses: Residues from eclogite melting experiments (Carroll and Wyllie 1990; Winther and Newton 1991; Sen and Dunn 1994; Rapp and Watson 1995), assuming equal proportions of residual garnet and cpx. Purple stars: oceanic gabbros (Casey 1997; Perk et al. 2007; Godard et al. 2009). Triangles: oceanic olivine gabbro (Casey 1997; Perk et al. 2007; Godard et al. 2009). Yellow field outlines data for Archean cratonic basalts and pink field outlines Archean picrite; dark blue field is for basalt from Archean greenstone belt (data from PetDB and geochemical rock database (Lehnert et al. 2000)). Green and purple fields are eclogites from Udachnaya (Agashev et al. 2018; Sobolev et al. 1994) and Mir (Beard et al. 1996; Snyder et al. 1997) kimberlites, respectively. Experimental pyrolite melts (red symbols) at 1, 3 and 4 GPa, respectively (Baker and Stolper 1994; Walter 1998)

degrees (Harte 1987). Therefore, it is important to evaluate the effects of metasomatic processes on the primary compositions of these xenoliths.

Several lines of evidence suggest that most eclogites in this study have not been strongly metasomatized: (1) phlogopite and amphibole, which are typically added to the cratonic mantle during modal metasomatism (e.g., eclogites from Kimberley, Kaapvaal craton; Jacob et al. 2009; Shu et al. 2018), are not observed in eclogites in this study. (2) Interaction with low-volume alkaline melts can lead to TiO_2 and high field-strength element (HFSE) enrichment in garnet (e.g., Pearce 2008). Garnets from the Obnazhennaya eclogites do not show evidence for such melt-rock interaction. (3) Melt metasomatism is expected to increase the concentrations of most incompatible elements, like LREE, contents of the original eclogite (Ireland et al. 1994) and results in $(La/Yb)_N > 1$. While many of the samples analyzed here show LREE-enrichment ($(La/Yb)_N > 1$), which may be due to late-stage metasomatism, the enrichment appears to be confined to the lightest REE and does not extend into the MREE. Interpolating from the MREE–HREE, one can see that all samples in this study were originally LREE-depleted. The exception, sample O-927 from the previous study of Taylor et al. (2003), has a $(La/Yb)_N$ ratio of 1.8 (Fig. 4), which may reflect metasomatic overprinting. This sample has lower FeO and higher Mg#, which could be due to small degrees of metasomatic overprint after partial melting or metasomatism. However, partial melting will also result in strong depletion of SiO_2, but the sample has the highest SiO_2 of all of the low-MgO Obnazhennaya eclogites. Combined with its enriched LREE pattern, we, therefore, favor metasomatism as an explanation for the low FeO and high SiO_2 content and Mg# for this sample. Hence, sample O-927 will be omitted from further discussion.

Origin of the low-MgO eclogites

Low-MgO eclogite xenoliths have been reported from South Africa (e.g., Gréau et al. 2011; Huang et al. 2012, 2014; Shu et al. 2013), Finland (Peltonen et al. 2002; Smart et al. 2017a), West Africa (e.g., Hills and Haggerty 1989; Fung and Haggerty 1995; Barth et al. 2001; Aulbach and Arndt 2019), the Slave craton (e.g., Aulbach et al. 2007; Smart et al. 2012, 2014, 2017b) and Udachnaya (Agashev et al. 2018) and Mir (Snyder et al. 1997) in Siberia. Here, we evaluate models for the origin for the Obnazhennaya low-MgO eclogites: (1) as cumulates from mafic melts at higher pressures ("mantle" hypothesis) (Caporuscio and Smyth 1990; and references therein); (2) as residues from partial melting of subducted Archean basalts (Ireland et al. 1994; Barth et al. 2001); (3) as foundered lower continental crust (Hills and Haggerty 1989; Pearson et al. 1991); (4) as foundered or subducted low-pressure cumulates that may or may not have experienced partial melting (Barth et al. 2002; and references therein). We evaluate each of these hypotheses, in turn.

High-pressure cumulates from mantle melts?

According to the "mantle" hypothesis, the eclogites should have oxygen isotopic compositions similar to those of primary mantle melts or their cumulates that formed at pressures exceeding 3 GPa (e.g., Hatton 1978). Most low-MgO eclogites from Obnazhennaya have equilibration pressures

Table 7 Major element composition (wt%) of reconstruct clinopyroxene from the Obnazhennaya eclogites

	Vol	SiO_2	TiO_2	Al_2O_3	Cr_2O_3	FeO	MnO	MgO	CaO	Na_2O	K_2O	NiO	Total	Jd	Mg#	CaTs
7-303																
Host cpx	0.75	53.76	0.11	6.32	0.05	2.96	0.01	13.16	19.62	2.93	0.01	0.05	98.99	0.21	0.89	0.00
Grt lamella	0.25	40.00	0.01	22.21	0.06	12.57	0.34	10.30	13.37	0.01	0.00	0.01	98.87			
Reconstruct cpx		50.32	0.09	10.29	0.05	5.36	0.09	12.45	18.06	2.20	0.01	0.04	98.96	0.18	0.81	0.13
7-350																
Host cpx	0.73	53.30	0.14	6.17	0.04	2.61	0.04	13.44	17.62	3.25	0.01	0.12	96.72	0.25	0.90	0.01
Grt lamella	0.27	40.45	0.03	22.81	0.05	11.44	0.22	17.91	3.53	0.01	0.00	0.02	96.48			
Reconstruct cpx		49.83	0.11	10.66	0.04	4.99	0.09	14.65	13.82	2.37	0.01	0.09	96.66	0.24	0.84	0.14
7-354																
Host cpx	0.80	53.14	0.08	6.98	0.05	2.93	0.02	12.73	19.14	3.02	0.01	0.07	98.18	0.22	0.89	0.04
Grt lamella	0.20	39.76	0.04	22.08	0.03	11.97	0.28	8.96	15.45	0.01	0.01	0.01	98.60			
Reconstruct cpx		50.46	0.07	10.00	0.05	4.74	0.07	11.98	18.40	2.42	0.01	0.06	98.26	0.19	0.82	0.12
7-379																
Host cpx	0.70	53.30	0.18	6.46	0.08	3.03	0.02	13.02	19.12	3.03	0.00	0.06	98.30	0.22	0.89	0.02
Grt lamella	0.30	39.92	0.02	22.45	0.07	12.99	0.35	11.94	10.64	0.02	0.01	0.01	98.41			
Reconstruct cpx		49.29	0.13	11.26	0.08	6.02	0.12	12.70	16.57	2.12	0.01	0.05	98.34	0.19	0.79	0.16
7-394																
Host cpx	0.95	51.53	0.05	15.39	0.05	1.12	0.00	8.90	17.66	4.44	0.01	0.13	99.28	0.31	0.93	0.23
Grt lamella	0.05	41.81	0.03	23.63	0.07	5.49	0.09	9.37	21.13	0.02	0.00	0.00	101.64			
Reconstruct cpx		51.09	0.05	15.77	0.05	1.32	0.01	8.92	17.82	4.24	0.01	0.12	99.39	0.30	0.92	0.20
74-136																
Host cpx	0.92	53.17	0.09	6.20	0.04	3.54	0.02	13.02	19.70	2.67	0.00	0.04	98.49	0.20	0.87	0.03
Grt lamella	0.08	39.80	0.03	22.32	0.04	14.22	0.32	9.18	13.61	0.01	0.00	0.01	99.53			
Reconstruct cpx		52.11	0.08	7.47	0.04	4.38	0.04	12.71	19.22	2.46	0.00	0.04	98.57	0.19	0.84	0.06
74-639																
Host cpx	0.97	53.76	0.04	6.15	0.01	3.21	0.03	13.39	19.85	2.67	0.01	0.05	99.17	0.20	0.88	0.00
Grt lamella	0.03	39.68	0.02	22.22	0.01	13.28	0.37	10.30	12.77	0.02	0.00	0.00	98.66			
Reconstruct cpx		53.31	0.04	6.66	0.01	3.53	0.04	13.29	19.63	2.59	0.01	0.05	99.16	0.19	0.87	0.04

between 3.0 and 3.7 GPa (Fig. 6) and mantle-like oxygen isotopic compositions (Fig. 5), which seems to be consistent with the hypothesis. However, the major element compositions of the Obnazhennaya low-MgO eclogites differ significantly from primary and high-pressure mantle melts (Fig. 7). Picritic melts generated between 3 and 4 GPa have higher MgO and lower CaO contents than the Obnazhennaya low-MgO eclogites. Picritic melts derived from relative lower pressures, i.e., at 1 GPa, have moderate MgO content (10–16 wt%) that overlap well with the low-MgO eclogites. However, these melts show constant SiO_2 (~ 50 wt%) and CaO (11–13 wt%) contents at different MgO compositions, while the low-MgO Obnazhennaya eclogites display negative correlations between CaO vs. MgO and SiO_2 vs. MgO contents. Such negative correlations in the low-MgO eclogites argue against their origin as crystallized low-pressure picritic melts. In addition, five out of eight Obnazhennaya samples in this study have Ni contents lower than primary mantle melts (208–311 ppm vs. ≥ 320 ppm, Frey et al. 1978), though sulfide is not considered in the reconstruction of the bulk rock, so the Ni contents discussed here are minimum values. Moreover, cumulates of garnet and cpx from primary mantle melts at pressures greater than 3 GPa (Walter 1998) cannot produce the positive Eu and Sr anomalies in our samples (Fig. 4a, b) and non-mantle-like oxygen isotopic compositions of sample 7-303 (4.73‰) in this study and samples in the previous study (7.1–7.8‰). Thus, the protoliths of the low-MgO Obnazhennaya eclogites are unlikely to be mantle melts crystallized at high pressures, nor high pressure cumulates.

Residues of altered and metamorphosed Archean basalt?

Most Obnazhennaya low-MgO eclogites have higher CaO, and Al_2O_3 but lower FeO and SiO_2 contents than Archean cratonic basalts (yellow field in Fig. 7), but partially overlap with basalts from Archean greenstone belts and also modern oceanic gabbros, especially for SiO_2 and MgO (Figs. 7, 8; Appendix 4) (Winther and Newton 1991; Sen and Dunn 1994; Rapp and Watson 1995). Similar findings were

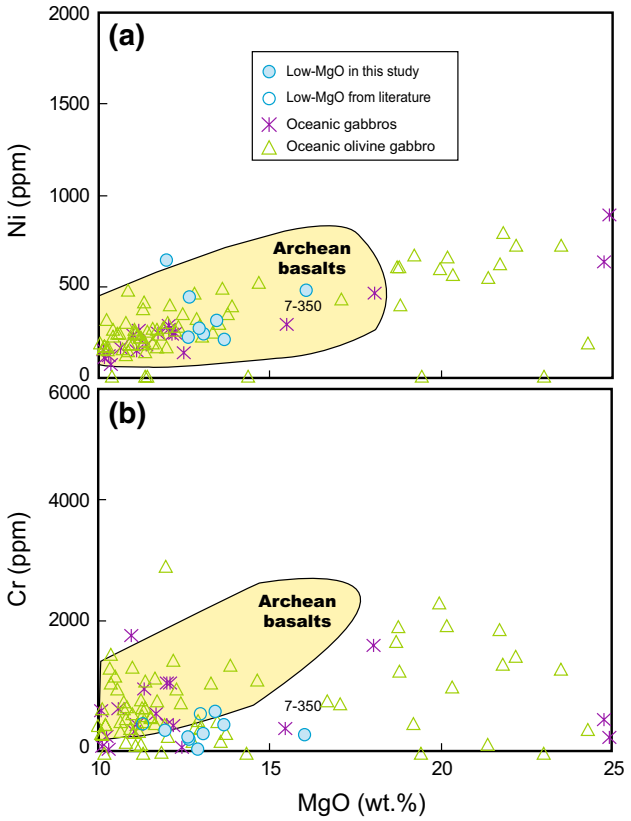

Fig. 8 Whole-rock MgO (wt%) vs. Ni (**a**) and Cr (**b**). Symbols and data sources as in Fig. 7

reported by previous studies, e.g., the low-MgO eclogites from the Koidu kimberlite (Barth et al. 2001) have lower SiO_2 and higher CaO contents than Archean basalts, but overlap with the residues of partial melting experiments of Archean basalt. Therefore, Barth et al. (2001) interpreted the Koidu low-MgO eclogites as residues of silica-rich melt extraction from Archean basalts. Similarly, Taylor et al. (2003) interpreted Obnazhennaya Group B eclogites as residues after the extraction of a TTG melt. However, low silica contents may result not only from partial melting, but also from seafloor alteration (Ridley et al. 1994; Staudigel et al. 1995; Hart et al. 1999). Indeed, the elevated $\delta^{18}O$ (7.1–7.8‰) of low-MgO Obnazhennaya eclogites from the previous study were interpreted to reflect low-T seafloor alteration. Hence, it is uncertain whether the samples depleted in SiO_2 in the previous study are the residues of Archean basalt partial melting. It seems that the protolith of some eclogites with the depleted SiO_2 can be residues from partial melting of Archean basalts. However, compared to the experimental melting residues of Archean basalt, most Obnazhennaya low-MgO eclogites from this study show higher MgO, CaO, and Al_2O_3 but lower FeO contents, (Figs. 7, 8; Appendix 4) (Winther and Newton 1991; Sen and Dunn 1994; Rapp and Watson 1995). Moreover, the positive slopes and high contents of the HREE in Obnazhennaya low-MgO eclogites (Fig. 4a) require the presence of large volumes of garnet in an open system—either during partial melting or during crystal accumulation. Therefore, the low-MgO Obnazhennaya eclogites are unlikely to be the residua of melting of Archean basalts.

Foundered lower continental crust?

Mafic granulites formed by crystallization of underplated basalts are typically encountered in the lower continental crust or near the crust–mantle boundary (Herzberg et al. 1983; O'Reilly and Griffin 2013). If such mafic rocks are tectonically buried, they could convert to eclogites, and founder to greater depths (Hills and Haggerty 1989; Pearson et al. 1991). Although P–T estimates indicate that Siberian eclogites and granulites do not exist at the same depths within the lithosphere (2.3–3.7 GPa vs. 0.8–1.2 GPa, respectively; Koreshkova et al. 2011; Moyen et al. 2017), it is conceivable that the Obnazhennaya low-MgO eclogites represent former lower continental crust that foundered to greater depths. However, this hypothesis cannot explain the mantle-like $\delta^{18}O$ values observed in most Obnazhennaya low-MgO eclogites in this study, because the Oxygen-isotope compositions of most mafic lower crustal granulites are elevated well above the mantle value due to the assimilation of pre-existing lower crust (Fowler and Harmon 1990; Kempton and Harmon 1992).

Low-pressure cumulate protoliths?

As discussed above, the low-MgO Obnazhennaya eclogites do not have the compositions of Archean basalts (Figs. 7, 8), suggesting that they do not represent liquid compositions. By contrast, they have relatively high MgO contents and significant positive Eu anomalies in both calculated bulk rocks and minerals (Figs. 3, 4), which point toward a low-pressure cumulative origin, where plagioclase was a stable phase. Reconstructed bulk rocks show an anti-correlation between Eu/Eu* and ∑HREEs (Appendix 5), which is consistent with plagioclase accumulation (Aulbach and Arndt 2019). Normative plagioclase (43%), diopside (27%) and olivine (23%) are similar to modes of (olivine) gabbroic cumulate rocks from modern MORB (Appendix 1). However, the reconstructed bulk rock compositions of the low-MgO eclogites have lower SiO_2 and higher CaO and MgO contents compared to oceanic gabbros. Such offset can be attributed to differences in the composition of their parental melts, or to later melt extraction (Fig. 7). When compared with pyrolite melts from different pressures (1 GPa, 3 Gpa and 4 GPa; Walter 1998), most low-MgO eclogites (except 7-350 and two eclogites in the previous study) are depleted

in SiO_2 and enriched in CaO and also Al_2O_3 (Fig. 7), which could also reflect partial melting and extraction of silicic melts. The low-MgO eclogites are also depleted in LREE with $(Nd/Yb)_N$ ratios < 1, again consistent with partial melt extraction after protolith formation (Aulbach and Arndt 2019).

Therefore, we modeled the trace elements to test the hypothesis that low-MgO eclogites originated as melt residues of low-pressure cumulates. Although the age of Obnazhennaya eclogites is not known, two point Sm–Nd isochrons of garnet–clinopyroxene mineral pairs yield ages of 1.2 Ga, which suggest they are at least Mesoproterozoic in age (Taylor et al. 2003). The ambient mantle temperature earlier in Earth history is much hotter than in the modern time, which results in the difference in composition between Archean basalt and modern MORB (Herzberg et al. 2010). Archean basalt is more Mg-rich (MgO > 10%) than modern MORB (average MgO = 7.6%; Gale et al. 2013). Therefore, Archean basalts were used as the parental melt from which the low-pressure cumulates precipitate (with or without trapped melt). REE and Sr relative concentrations (Fig. 9) suggest the low-pressure (≤ 0.5 GPa) accumulation of olivine, plagioclase, and clinopyroxene for all of the low-MgO Obnazhennaya samples (cf. Presnall et al. 1978). Model parameters are given in the caption of Fig. 9.

The composition of sample 7-350, with the lowest HREE contents (Lu = 0.6 × chondrite), the highest LREE content, and the largest positive Sr and Eu anomalies, is clearly indicative of a low-pressure, plagioclase-rich cumulate origin. The flat light to middle REE pattern suggests that this sample may not have experienced partial melting. Based on our calculations (Fig. 9a), a mixture of 50% plagioclase, 30% olivine, and 20% clinopyroxene cumulate can reproduce the eclogite composition. This is supported by the calculated CIPW norm which shows 48% plagioclase for this sample (Appendix 1). The trace-element composition of minerals for the model cumulate are taken from an olivine gabbro sample from IODP Site U1309 (Godard et al. 2009), which has a similar major element composition as 7-350 in this study. The $(Nd/Yb)_N$ ratio of such a cumulate is 0.92, matching the ratio of the sample 7-350 (1.0) and the two eclogites (O-82/91, O-501) in the previous study of Taylor et al. (2003) with $(Nd/Yb)_N$ ratios 0.91 and 0.96, respectively (Fig. 9a). These three samples have similar REE patterns as the low-pressure cumulate, but higher overall REE contents. We, therefore, mix variable amounts of Archean basalt with the cumulate melt to reproduce these three eclogite compositions. The compositions are successfully explained if the nonmodal batch melt is allowed to vary from 5 to 20% (Fig. 9a).

For samples with depleted features, e.g., low incompatible element and high and fractionated HREE, we used a fractional melting model of subducted basalt at different pressures to determine how the partial melting process affects the chemical compositions of the low-MgO Obnazhennaya eclogites and to determine whether any constraints can be placed on the degrees and depths of partial melting. The average composition of modern-day oceanic gabbro (Casey 1997) is used as the starting composition (M1) for our model. The sample was melted in both the garnet and plagioclase stability field. Our calculations show that partial melting will not generate the observed positively sloped patterns for middle to heavy REE if the starting materials do not contain garnet. Instead it will generate negatively sloped HREE patterns and will significantly lower the HREE contents (Fig. 9b). However, repeated/continuous melting in the eclogite stability field with different mineral modal abundances will produce the higher and fractionated HREE pattern similar to out samples (Fig. 9c). We assume that different stages of partial melting affected these eclogites before they were brought back to the surface: Stage 1: 15% melting of eclogite with the composition of M1, mineral modal abundance ratios: grt/cpx = 60:40. The residue composition is M2; Stage 2: use M2 as a starting material, calculate 20% melt loss; grt/cpx ratio in the residue is 65:35. The residue composition is M3; Stage 3: use M3 as a starting material, remove another 20% of melt; grt/cpx ratio will be 70:30. The residue composition is then M4. Stage 4: starting with M4, remove another 20% of melt; grt/cpx ratio will be 75:25. The residue composition is M5. Stage 5: starting with M5, remove another 20% of melt; grt/cpx ratio will be 20:80, and M6 is the residue composition. The melting modal for our calculation has Grt/cpx ratio of 60/40 (details for modeling calculation are present in Appendix 1). The $(Dy/Yb)_N$ ratios of the residues, M1, M2, M3, M4, M5 and M6, are 0.91, 0.86,0.80, 0.75, 0.70, 0.66, respectively (Fig. 9c; Appendix 1). They compare well with the low-MgO eclogites having fractionated HREE patterns (from 0.58 to 0.93). Continuous or repeated melting decreases cpx and increases the garnet modal abundance in the residues. This is constituent with the high modal garnet abundance in the sample suite.

Despite the successful match of the HREE fractionation between our model calculations and the low-MgO eclogites when using the average composition of MORB gabbro as starting material, a number of our samples have similarly fractionated patterns but higher HREE–MREE contents ($(Lu)_N$ = 4–10 times Chondrite). When adding 10% Archean basaltic melt into the average composition of modern oceanic gabbro, the REE pattern and contents overlap well with these samples (Fig. 9c). Therefore, continuous partial melting of the low-MgO Obnazhennaya eclogites likely occurred in the eclogite stability field, after the cumulates (some with trapped melt) were brought to high pressures. Repeated melting of eclogite in the lithospheric mantle has also been explored by experimental studies (e.g., Rosenthal

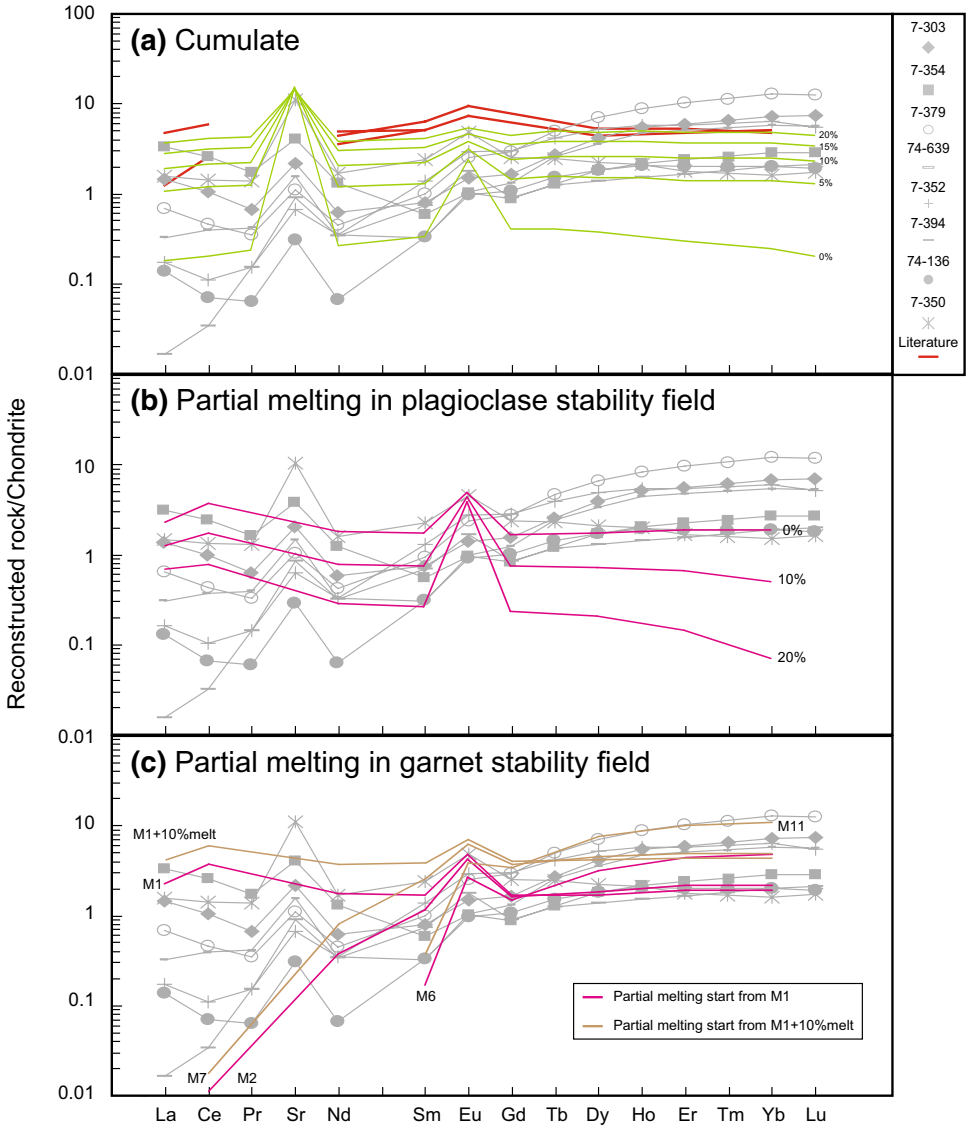

Fig. 9 **a** Low-MgO eclogites interpreted to be low-pressure cumulates are shown in grey. Green lines are a calculated ol-plag-cpx cumulate in equilibrium with an olivine gabbro from IODP Site U1309 (Godard et al. 2009) containing 0–20% Archean basalt. The cumulate consists of 50% plagioclase, 30% olivine, and 20% clinopyroxene, comparable to the CIPW norms of the sample 7–350. Red lines are low-MgO Obnazhennaya eclogites from Taylor et al. (2003). **b** Model calculations for various degrees of batch partial melting in plagioclase stability field. The starting composition is using the composition of gabbro from modern ocean (Casey 1997) and starting minerals are 50% plagioclase, 20% olivine and 30% clinopyroxene comparable to the average CIPW norms of the low-MgO Obnazhennaya eclogites. Pink lines are calculated compositions of variable degree partial melting. Numbers give the percentage of partial melting degree. **c** Model calculations for fractional partial melting in the eclogite stability field. Pink and light brown lines are calculated compositions of episode partial melting using M1 and M1 + 10% melt as starting material. M1 is the same gabbro composition as the starting material used in **b**. M1 + 10% melt is the M1 with 10% Archean basalts. M2 and M7 is 15% of melting with the starting composition of M1 and M1 + 10% melt, respectively. M6 and M11 is the residue of the fifth partial melting. Detail calculate description is provided in Appendix 1

et al. 2014), and was proposed as an important mechanism to cause refertilization and compositional heterogeneity of the upper mantle.

In summary, based on the major and trace-element compositions of low-MgO Obnazhennaya eclogites in this study, their protoliths can be explained as plagioclase-dominated cumulates formed at low pressure that repeatedly partially melted to variable degrees after eclogite metamorphism.

Oxygen isotopic features

The $\delta^{18}O$ of modern ocean floor lithologies are significantly more variable than that of the mantle ($5.5 \pm 0.4‰$; Mattey et al. 1994). Heavier $\delta^{18}O$ values than that of the mantle are observed in sea floor basalts altered at relatively low temperature, while lighter $\delta^{18}O$ values reflect high-temperature seafloor alteration in the lower parts of the oceanic crust (e.g., Gregory and Taylor 1981; McCulloch et al. 1981). Although Huang et al. (2014) attributed variable $\delta^{18}O$ in eclogites from Roberts Victor, South Africa to melt metasomatism, we observe no correlation between $\delta^{18}O$ of the low-MgO eclogites with incompatible trace elements, ruling out the metasomatism scenario. Therefore, we only consider seawater–rock exchange to explain the eclogite $\delta^{18}O$ values.

The $\delta^{18}O$ values of garnets from two Obnazhennaya eclogites in the previous study of Taylor et al. (2003) (7.1–7.8‰) are significantly heavier than the mantle value, which was attributed to low-temperature seafloor alteration. In addition, the garnet from sample 7-303 in our sample suite with lower $\delta^{18}O$ values (4.73‰) also suggests a high-temperature seafloor alteration. Such alteration can also cause depletions of CaO and of SiO_2, which is consistent with the lower CaO and SiO_2 content of these three samples relative to samples in this study.

It remains unclear if the protoliths of most Obnazhennaya low-MgO eclogites with mantle-like $\delta^{18}O$ were hydrothermally altered. Either the protoliths did not interact with seawater, or such interaction coincidently produced normal igneous values. In the lowermost oceanic crust, hydrothermal alteration is localized along fractures and veins (Gregory and Taylor 1981; Dick et al. 2000). Thus, it is possible that most of the protoliths of the eclogites in this study did not experience hydrothermal alteration. Alternatively, seawater-derived hydrothermal fluids have variable $\delta^{18}O$, and a gabbro can be hydrothermally altered over a significant range of temperatures to produce a $\delta^{18}O$ value that is coincidentally consistent to the mantle value (Barth et al. 2002). Moreover, if the cumulate formed deep within in a thicker oceanic crust, hydrothermal processes may not reach these depths, even at fractures generated by bending plates.

Geological implications

If the Obnazhennaya eclogites are the products of low-pressure crystal accumulation and subduction of thermally equilibrated ancient oceanic crust, then a transient heating event must be postulated to produce the high temperatures at 2 GPa. This may occur during a rifting event at the edge of the craton, generating the high-temperature eclogites, followed by cooling and garnet exsolution.

Alternatively, the history of the low-MgO Obnazhennaya eclogite xenoliths may be as follows (Fig. 10): (1) accumulation of ol, cpx and plag at somewhat elevated pressure, i.e., ~ 0.5 GPa deep within a thick Archean oceanic crust, where high temperatures are preserved for a longer time; (2) subduction of the hot cumulate and metamorphism at high temperature to generates first s high-T mafic granulites and the high-T eclogites with Al-rich cpx; and (3) secular cooling to ambient mantle conditions or pressure increasing causing exsolution of garnets.

Eclogite xenoliths from several kimberlites (e.g., Udachnaya, Mir) located within the Siberian craton have been previously studied. Compared with low-MgO (Group B/C) eclogite xenoliths from Udachnaya and Mir kimberlite, samples from the Obnazhennaya kimberlite have comparable major, trace elements, (including positive Eu anomalies), and oxygen isotopic characteristics, which indicate their oceanic crust origin. However, most garnets from the Obnazhennaya eclogites show mantle-like oxygen isotopic ratios relative to those from the Udachnaya (4.9–7.0‰; Jacob et al. 1994; Shatsky et al. 2016) and Mir kimberlites (3.1–7.2‰; Beard et al. 1996). Additionally, Obnazhennaya low-MgO eclogite xenoliths have systematically lower LREE and incompatible elements than those from Udachnaya and Mir. These differences may reflect that the Udachnaya and Mir kimberlite pipes lie near the center of the Siberian craton, and thus could have tapped a source from deeper in the mantle keel. By contrast, Obnazhennaya kimberlite pipe is located on the edge of craton; therefore, their eclogite xenoliths remained at relative lower temperature within the mantle.

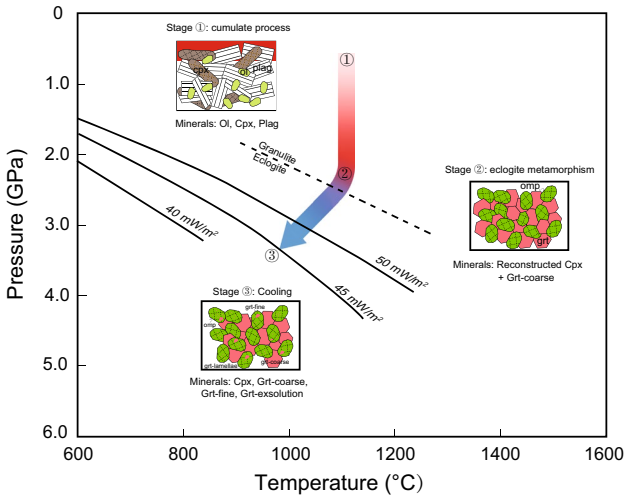

Fig. 10 Schematic representation of the possible formation processes of the Obnazhennaya low-MgO eclogites suite

Summary and conclusions

The low-MgO eclogites from the Obnazhennaya kimberlite pipe in Yakutia offer the rare occasion to deduce their protoliths from their geochemical properties but also to reconstruct the path that led to their transformation to eclogites using the garnet exsolution lamellae in their clinopyroxenes.

(1) Petrographic and geochemical features of the Obnazhennaya low-MgO eclogite xenoliths in our study revealed a somewhat different petrogenesis than suggested in the previous study of Taylor et al. (2003). Our findings are consistent with an origin as subducted or foundered oceanic crust, as proposed by Taylor et al. (2003), but we suggest that the protoliths of low-MgO eclogite xenoliths were oceanic olivine gabbro cumulates with or without trapped melt that later partially melted, rather than basaltic oceanic crust.

(2) The low-MgO eclogites from Obnazhennaya contain two types of garnet with different compositions: granular coarse garnet and garnet exsolution (lamellae and fine-grained) in clinopyroxene. Pressures and temperatures calculated from the last stage of equilibrium phases (garnet lamellae and their host clinopyroxene) suggest that the eclogites were derived from between 855 and 1095 °C and 2.3–3.7 GPa. By contrast, the coarse garnet and reconstructed clinopyroxene give an average about 2 GPa and a range of temperatures between 1000 and 1200 °C. Thus, the eclogites were brought to greater depths as they cooled.

(3) Ratios of $(Nd/Yb)_N < 1$ and positively slopped HREE ($(Dy/Yb)_N < 1$) in most eclogites require repeated partial melting in the eclogite stability field.

Acknowledgements The authors profited from continuous help and support in the laboratory and through discussions with John Valley (University of Wisconsin, SIMS), Michael Spicuzza (WiscSIMS), Liangliang Zhang (China University of geosciences, Beijing) and Qin Zhou (National Astronomical Observatories, Chinese Academic of Sciences). Constructive reviews by Sonja Aulbach and an anonymous reviewer are greatly appreciated. This study was financially supported by the major national science and technology projects (2017ZX05063002-006) and by NSF-EAR-1650260 (to RLR). Part of the analytical work and the writing of this paper was carried out by Jing Sun when she was a visiting scholar at UC Santa Barbara. Her visit was funded by the China Scholarship Council. WiscSIMS is supported by NSF-EAR-1658823 and the University of Wisconsin-Madison.

References

Agashev AM, Pokhilenko LN, Pokhilenko NP, Shchukina EV (2018) Geochemistry of eclogite xenoliths from the Udachnaya kimberlite pipe: section of ancient oceanic crust sampled. Lithos 314–315:187–200

Alifirova TA, Pokhilenko LN, Ovchinnikov YI, Donnelly CL, Riches AJV, Taylor LA (2012) Petrologic origin of exsolution textures in mantle minerals: evidence in pyroxenitic xenoliths from Yakutia kimberlites. Int Geol Rev 54(9):1071–1092

Alifirova TA, Pokhilenko LN, Korsakov AV (2015) Apatite, SiO_2, rutile and orthopyroxene precipitates in minerals of eclogite xenoliths from Yakutian kimberlites, Russia. Lithos 226:31–49

Armstrong JT (1995) CITZAF-A package of correction programs for the quantitative electron microbeam X-ray-analysis of thick polished materials, thin-films, and particles. Microbeam Anal 4(3):177–200

Aulbach S, Arndt NT (2019) Eclogites as palaeodynamic archives: evidence for warm (not hot) and depleted (but heterogeneous) Archaean ambient mantle. Earth Planet Sci Lett 505:162–172

Aulbach S, Jacob DE (2016) Major- and trace-elements in cratonic mantle eclogites and pyroxenites reveal heterogeneous sources and metamorphic processing of low-pressure protoliths. Lithos 262:586–605

Aulbach S, Stagno V (2016) Evidence for a reducing Archean ambient mantle and its effects on the carbon cycle. Geology 44(9):751–754

Aulbach S, Pearson N, O'Reilly SY, Doyle BJ (2007) Origins of xenolithic eclogites and pyroxenites from the central Slave craton. Can J Petrol 48(10):1843–1873

Aulbach S, Höfer HE, Gerdes A (2019) High-Mg and low-Mg mantle eclogites from Koidu (West African craton) linked by Neoproterozoic ultramafic melt metasomatism of subducted Archaean plateau-like oceanic crust. J Petrol 60(4):723–754

Baker MB, Stolper EM (1994) Determining the composition of high-pressure mantle melts diamond aggregates. Geochim Cosmochim Acta 58:2811–2827

Barth MG, Rudnick RL, Horn I, McDonough WF, Spicuzza MJ, Valley JW, Haggerty SE (2001) Geochemistry of xenolithic eclogites from West Africa, Part I: a link between low MgO eclogites and Archean crust formation. Geochim Cosmochim Acta 65(9):1499–1527

Barth MG, Rudnick RL, Horn I, McDonough WF, Spicuzza MJ, Valley JW, Haggerty SE (2002) Geochemistry of xenolithic eclogites from West Africa, part 2: origins of the high MgO eclogites. Geochim Cosmochim Acta 66(24):4325–4345

Beard BL, Fraracci KN, Taylor LA, Snyder GA, Clayton RA, Mayeda TK, Sobole NV (1996) Petrography and geochemistry and eclogites from the Mir kimberlite, Yakutia, Russia. Contrib Mineral Petrol 125:293–310

Beck R (1907) Untersuchungen uber einige sudafrikanische diamantlagerstatten. Z Dtsch Geol Ges 59:275–307

Beyer C, Frost DJ, Miyajima N (2015) Experimental calibration of a garnet–clinopyroxene geobarometer for mantle eclogites. Contrib Mineral Petrol 169(2):18. https://doi.org/10.1007/s00410-015-1113-z

Blanco D, Kravchinsky VA, Konstantinov KM, Kabin K (2013) Paleomagnetic dating of Phanerozoic kimberlites in Siberia. J Appl Geophys 88(1):139–153

Caporuscio FA, Smyth JR (1990) Trace element crystal chemistry of mantle eclogites. Contrib Mineral Petrol 105:550–561

Carroll MR, Wyllie PJ (1990) The system tonalite-H_2O at 15 kbar and the genesis of calc-alkaline magmas. Am Mineral 75(3–4):345–357

Casey J (1997) Comparison of major-and trace-element geochemistry of abyssal peridotites and mafic plutonic rocks with basalts from the MARK region of the Mid-Atlantic Ridge. Proc Oceab Drill Prog Sci Result 153:181–241

Chapman DS, Pollack HN (1977) Regional geotherms and lithospheric thicknesses. Geology 5:265–268

Clark JR, Appleman DE, Papike JJ (1968) Bonding in eight ordered clinopyroxenes isostructural with diopside. Contrib Mineral Petrol 20(1):81–85

Davis GL, Sobolev NV, Khar'Kiv AD (1980) New data on the age of Yakutian kimberlites obtained by the uranium-lead on zircons. Dokl Akad Nauk SSSR 254:175–180

Deines P, Haggety SE (2000) Small-scale oxygen isotope variations and petrochemistry of ultradeep (%3e 300 km) and transition zone xenoliths. Geochim Cosmochim Acta 64:117–131

Deines P, Harris JW, Robinson DN, Gurney JJ, Shee SR (1991) Carbon and oxygen isotope variations in diamond and graphite eclogites from Orapa, Botswana, and the nitrogen content of their diamonds. Geochim Cosmochim Acta 55:515–524

Dick HJ, Natland JH, Alt JC, Bach W, Bideau D, Gee JS, Haggas S, Hertogen JG, Hirth G, Holm PM (2000) A long in situ section of the lower ocean crust: results of ODP leg 176 drilling at the southwest Indian Ridge. Earth Planet Sci Lett 179(1):31–51

Dobosi G, Kurat G, Wall F (2007) Trace element fractionation during exsolution of garnet from clinopyroxene in an eclogite xenolith from Obnazhennaya (Siberia). Geochim Comochim Acta 71(15):227–227

Farver JR (2010) Oxygen and hydrogen diffusion in minerals. Rev Mineral Geochem 72(1):447–507

Fowler MB, Harmon RS (1990) The oxygen isotope composition of lower crustal granulite xenoliths. In: Vielzeuf D, Vidal P (eds) Granulites and crustal evolution. NATO ASI series (series C: mathematical and physical sciences), 311st edn. Springer, Dordrecht, pp 493–506

Frey FA, Green DH, Roy SD (1978) Integrated models of basalt petrogenesis: a study of quartz tholeiites to olivine melilitites from south eastern Australia utilizing geochemical and experimental petrological data. J Petrol 19(3):463–513

Fung AT, Haggerty SE (1995) Petrography and mineral compositions of eclogites from the Koidu Kimberlite Complex, Sierra Leone. J Geophys Res Solid Earth 100:20451–20473

Gale A, Dalton CA, Langmuir CH (2013) The mean composition of ocean ridge basalts. Geochem Geophys Geosyst 14(3):489–518

Gasparik T (1984) Experimentally determined stability of clinopyroxeneegarnet + corundum in the system CaO–MgO–Al_2O_3–SiO_2. Am Mineral 69:1025–1035

Godard M, Awaji S, Hansen H, Hellebrand E, Brunelli D, Johnson K, Yamasaki T, Maeda J, Abratis M, Christie D (2009) Geochemistry of a long in-situ section of intrusive slow-spread oceanic lithosphere: results from IODP Site U1309 (Atlantis Massif, 30 N Mid-Atlantic-Ridge). Earth Planet Sci Lett 279(1–2):110–122

Gréau Y, Huang JX, Griffin WL, Renac C, Alard O, O'Reilly SY (2011) Type I eclogites from Roberts Victor kimberlites: products of extensive mantle metasomatism. Geochim Cosmochim Acta 75(22):6927–6954

Gregory RT, Taylor HP (1981) An oxygen isotope profile in a section of Cretaceous oceanic crust, Samail Ophiolite, Oman: evidence for $\delta^{18}O$ buffering of the oceans by deep (%3e 5 km) seawater-hydrothermal circulation at mid-ocean ridges. J Geophys Res Solid Earth 86(B4):2737–2755

Griffin WL, Ryan CG, Kaminsky FV, O'Reilly SY, Natapov LM, Win TT, Kinny PD, Ilupin IP (1999) The Siberian lithosphere traverse: mantle terrances and the assembly of the Siberian Craton. Tectonophysics 310:1–35

Hart SR, Blusztajn J, Dick HJB, Meyer PS, Muehlenbachs K (1999) The fingerprint of seawater circulation in a 500-meter section of ocean crust gabbros. Geochim Cosmochim Acta 63(23):4059–4080

Harte B (1987) Metasomatic events recorded in mantle xenoliths: an overview. Mantle xenoliths, New York, pp 625–640

Harte B, Gurney JJ (1975) Evolution of clinopyroxene and garnet in an eclogite nodule from the Roberts Victor kimberlite pipe, South Africa. Phys Chem Earth 9:367–387

Hatton CJ (1978) The geochemistry and origin of xenoliths from the Roberts Victor mine. Ph.D thesis, University of Cape Town.

Herzberg C, Fyfe W, Carr M (1983) Density constraints on the formation of continental Moho and crust. Contrib Mineral Petrol 84(1):1–5

Herzberg C, Condie K, Korenaga J (2010) Thermal history of the Earth and its petrological expression. Earth Planet Sci Lett 292:79–88

Hills DV, Haggerty SE (1989) Petrochemistry of eclogites from the Koidu kimberlite complex, Sierra Leone. Contrib Mineral Petrol 103(4):397–422

Howarth GH, Barry PH, Pernet-Fisher JF, Baziotis IP, Pokhilenko NP, Pokhilenko LN, Bodnar RJ, Taylor LA, Agashev AM (2014) Superplume metasomatism: evidence from Siberian mantle xenoliths. Lithos 184–187(1):209–224

Huang JX, Gréau Y, Griffin WL, O'Reilly SY, Pearson NJ (2012) Multi-stage origin of Roberts Victor eclogites: progressive metasomatism and its isotopic effects. Lithos 142–143:161–181

Huang JX, Griffin WL, Gréau Y, Pearson NJ, O'Reilly SY, Cliff J, Martin L (2014) Unmasking xenolithic eclogites: progressive metasomatism of a key Roberts Victor sample. Chem Geol 364:56–65

Ireland TR, Rudnick RL, Spetsius Z (1994) Trace elements in diamond inclusions from eclogites reveal link to Archean granites. Earth Planet Sci Lett 128(3–4):199–213

Jacob DE, Foley SF (1999) Evidence for Archean ocean crust with low high field strength element signature from diamondiferous eclogite xenoliths. Lithos. https://doi.org/10.1016/S0024-4937(99)00034-1

Jacob D, Jagoutz E, Lowry D, Mattey D, Kudrjavtseva G (1994) Diamondiferous eclogites from Siberia: remnants of Archean oceanic crust. Geochim Cosmochim Acta 58(23):5191–5207

Jacob D, Bizimis M, Salters V (2005) Lu–Hf and geochemical systematics of recycled ancient oceanic crust: evidence from Roberts Victor eclogites. Contrib Mineral Petrol 148(6):707–720

Jacob DE, Viljoen KS, Grassineau NV (2009) Eclogite xenoliths from kimberley, South Africa—a case study of mantle metasomatism in eclogites. Lithos 112:1002–1013

Jerde EA, Taylor LA, Crozaz G, Sobolev NV (1993) Exsolution of garnet within clinopyroxene of mantle eclogites: major- and trace-element chemistry. Contrib Mineral Petrol 114:148–159

Kempton PD, Harmon RS (1992) Oxygen isotope evidence for large-scale hybridization of the lower crust during magmatic underplating. Geochim Cosmochim Acta 56(3):971–986

Kinny PD, Griffin B, Heaman L, Brakhfogel F, Spetsius ZV (1997) SHRIMP U-Pb ages of perovskite from Yakutian kimberlites. Russ Geol Geophys 38:97–105

Kitajima K, Strickland A, Spicuzza MJ, Tenner TJ, Valley JW (2016) Improved matrix correction of $\delta^{18}O$ analysis by SIMS for pyralspite and Cr-pyrope garnets. Goldschmidt Abstracts 1542

Koreshkova MY, Downes H, Levsky LK, Vladykin NV (2011) Petrology and geochemistry of granulite xenoliths from Udachnaya and Komsomolskaya kimberlite pipes. Sib J Petrol 52(10):1857–1885

Korolev NM, Melnik AE, Li XH, Skublov SG (2018) The oxygen isotope composition of mantle eclogites as a proxy of their origin and evolution: a review. Earth Sci Rev 185:288–300

Krogh REJ (1988) The garnet–clinopyroxene Fe–Mg geothermometer—a reinterpretation of existing experimental data. Contrib Miner Petrol 99(1):44–48

Krogh REJ (2000) The garnet–clinopyroxene Fe^{2+}–Mg geothermometer: an updated calibration. J Metamorph Geol 18:211–219

Lehnert K, Su Y, Langmuir CH, Sarbas B, Nohl U (2000) A global geochemical database structure for rocks. Geochem Geophys Geosyst 5(1):1–14

Mattey D, Lowry D, Macpherson C (1994) Oxygen isotope composition of mantle peridotite. Earth Planet Sci Lett 128(3–4):231–241

McCulloch MT, Gregory RT, Wasserburg G, Taylor HP (1981) Sm–Nd, Rb–Sr, and $^{18}O/^{16}O$ isotopic systematics in an oceanic crustal section: evidence from the Samail Ophiolite. J Geophys Res Solid Earth 86(B4):2721–2735

McDonough WF, Sun SS (1995) The composition of the Earth. Chem Geol 120(3–4):223–253

Morishita T, Arai S, Green DH (2004) Possible non-melted remnants of subducted lithosphere: experimental and geochemical evidence from corundum-bearing mafic rocks in the Horoman peridotite complex. Jpn J Petrol 45(2):235–252

Moyen JF, Paquette JL, Ionov DA, Gannoun A, Korsakov AV, Golovin AV, Moine BN (2017) Paleoproterozoic rejuvenation and replacement of Archaean lithosphere: evidence from zircon U–Pb dating and Hf isotopes in crustal xenoliths at Udachnaya, Siberian craton. Earth Planet Sci Lett 457:149–159

O'Hara M (1969) The origin of eclogite and ariegite nodules in basalt. Geol Mag 106(4):322–330

O'Reilly SY, Griffin WL (2013) Moho vs crust–mantle boundary: evolution of an idea. Tectonophysics 609:535–546

Page FZ, Kita NT, Valley JW (2010) Ion microprobe analysis of oxygen isotopes in garnets of complex chemistry. Chem Geol 270(1):9–19

Pearce JA (2008) Geochemical fingerprinting of oceanic basalts with applications to ophiolite classification and the search for Archean oceanic crust. Lithos 100(1):14–48

Pearson NJ, O'reilly SY, Griffin WL (1991) The granulite to eclogite transition beneath the eastern margin of the Australian craton. Eur J Mineral 3(2):293–322

Peltonen P, Kinnunen KA, Huhma H (2002) Petrology of two diamondiferous eclogite xenoliths from the Lahtojoki kimberlite pipe, eastern Finland. Lithos 63(3):151–164

Perk NW, Coogan LA, Karson JA, Klein EM, Hanna HD (2007) Petrology and geochemistry of primitive lower oceanic crust from Pito deep: implications for the accretion of the lower crust at the southern east Pacific rise. Contrib Mineral Petrol 154(5):575–590

Presnall DC, Dixon SA, Dixon JR, Donnel THO, Brenner NL, Schrock RL, Dycus DW (1978) Liquids phase relations on the join diopside–forsterite–anorthite from 1 atm to 20 kbar: their bearing on the generation and crystallization of basaltic magma. Contrib Mineral Petrol 66:203–220

Purwin H, Lauterbach S, Brey GP (2013) An experimental study of the Fe oxidation states in garnet and clinopyroxene as function of temperature in the system CaO–FeO–Fe_2O_3–MgO–Al_2O_3–SiO_2: implications for garnet–clinopyroxene geothermometry. Contrib Mineral Petrol 165:623–639

Qi Q, Taylor LA, Snyder GA, Sobolev NV (1994) Eclogites from the Obnazhennaya kimberlite pipe, Yakutia. Russ Int Geol Rev 36(10):911–924

Radu IB, Harris C, Moine BN, Costin G, Cotin JY (2019) Subduction relics in the subcontinental lithospheric mantle evidence from variation in the $\delta^{18}O$ value of eclogite xenoliths from the Kaapvaal craton. Contrib Mineral Petrol 174(3):19. https://doi.org/10.1007/s00410-019-1552-z

Rapp RP, Watson EB (1995) Dehydration melting of metabasalt at 8–32 kbar: implications for continental growth and crust-mantle recycling. J Petrol 36(4):891–931

Reiche M, Bautsch HJ (1985) Electron microscopical study of garnet exsolution in orthopyroxene. Phys Chem Miner 12:29–33

Ridley WI, Perfit MR, Jonasson IR, Smith MF (1994) Hydrothermal alteration in oceanic ridge volcanics: a detailed study at the Galapagos fossil hydrothermal field. Geochim Cosmochim Acta 58:2477–2494

Rosen OM, Condie KC, Natapov LM, Nozhkin AD (1994) Chapter 10 Archean and early Proterozoic evolution of the Siberian craton: a preliminary assessment. In: Condie KC (ed) Developments in Precambrian geology, vol 11. Amsterdam, pp 411–459

Rosenthal A, Yaxley GM, Green DH, Hermann J, Kovacs I, Spandler C (2014) Continuous eclogite melting and variable relertilisation in upwelling. Sci Rep 4:6099

Rudnick RL, Barth M, Horn I, McDonough WF (2000) Rutile-bearing refractory eclogites: missing link between continents and depleted mantle. Science 287:278–281

Schulze DJ (1989) Constraints on the abundance of eclogite in the upper mantle. J Geophys Res Solid Earth 94(B4):4205–4212

Sen C, Dunn T (1994) Dehydration melting of a basaltic composition amphibolite at 1.5 and 2.0 GPa: implications for the origin of adakites. Contrib Mineral Petrol 117(4):394–409

Shatsky VS, Zedgenizov DA, Ragozin AL (2016) Evidence for a subduction component in the diamond-bearing mantle of the Siberian craton. Russ Geol Geophys 57:111–126

Shu Q, Brey GP, Gerdes A, Hoefer EH (2013) Geochronological and geochemical constraints on the formation and evolution of the mantle underneath the Kaapvaal craton: Lu–Hf and Sm–Nd systematics of subcalcic garnets from highly depleted peridotites. Geochim Cosmochim Acta 113:1–20

Shu Q, Brey GP, Hoefer HE, Zhao Z, Pearson DG (2016) Kyanite/corundum eclogites from the Kaapvaal craton: subducted troctolites and layered gabbros from the mid- to early Archean. Contrib Mineral Petrol 171(2):11

Shu Q, Brey GP, Pearson DG (2018) Eclogites and garnet pyroxenites from Kimberley, Kaapvaal craton, South Africa: their diverse origins and complex metasomatic signatures. Mineral Petrol 112(1):43–56

Smart KA, Heaman LM, Chacko T, Simonetti A, Kopylova M, Mah D, Daniels D (2009) The origin of high-MgO diamond eclogites from the Jericho Kimberlite. Can Earth Planet Sci Lett 284(3–4):527–537

Smart KA, Chacko T, Stachel T, Tappe S, Stern RA, Ickert RB (2012) Eclogite formation beneath the northern Slave craton constrained by diamond inclusions: oceanic lithosphere origin without a crustal signature. Earth Planet Sci Lett 319–320(15):165–177

Smart KA, Chacko T, Simonetti A (2014) A record of Paleoproterozoic subduction preserved in the northern Slave cratonic mantle: Sr–Pb–O isotope and trace element investigations of eclogite xenoliths from the Jericho and Muskox kimberlites. J Petrol 55(3):549–583

Smart KA, Cartigny P, Tappe S (2017) Lithospheric diamond formation as a consequence of methane-rich volatile flooding: an example from diamondiferous eclogite xenoliths of the Karelian craton (Finland). Geochem Cosmochim Acta 206:312–342

Smart KA, Tappe S, Simonetti A (2017) Tectonic significance and redox state of Paleoproterozoic eclogite and pyroxenite components in the Slave cratonic mantle lithosphere, Voyageur kimberlite, Arctic Canada. Chem Geol 455:98–119

Smelov AP, Zaitsev AI (2013) The age and localization of kimberlite magmatism in the Yakutian kimberlite province: constraints from isotope geochronology—an overview. Springer, India, pp 225–234 https://doi.org/10.1007/978-81-322-1170-9_14

Snyder GA, Taylor LA, Crozaz G, Halliday AN, Beard BL, Sovolev VN, Sobolev N (1997) The origin of Yakutian eclogite xenoliths. J Petrol 38(1):85–113

Sobolev VN, Taylor LA, Snyder GA, Sobolev NV (1994) Diamondiferous eclogites from the Udachnaya kimberlite pipe, Yakutia, Siberia. Int Geol Rev 36:42–64

Spengler D, Alifirova T (2019) Formation of Siberian cratonic mantle websterites from high-Mg magma. Lithos 326–327:384–396

Staudigel H, Davies GR, Hart SR, Marchant KM, Smith BM (1995) Large scale isotopic Sr, Nd and O isotopic anatomy of altered oceanic crust: DSDP/ODP sites 417/418. Earth Planet Sci Lett 130(1):169–185

Sun J, Liu CZ, Tappe S, Kostrovitsky SI, Wu FY, Yakovlev D, Yang YH, Yang JH (2014) Repeated kimberlite magmatism beneath Yakutia and its relationship to Siberian flood volcanism: insights from in situ U–Pb and Sr–Nd perovskite isotope analysis. Earth Planet Sci Lett 404:283–295

Taylor LA, Snyder GA, Keller R, Remley DA, Anand M, Wiesli R, Valley J, Sobolev NV (2003) Petrogenesis of group A eclogites and websterites: evidence from the Obnazhennaya kimberlite, Yakutia. Contrib Mineral Petrol 145(4):424–443

Valley JW, Kitchen N, Kohn MJ, Niendorf CR, Spicuzza MJ (1995) UWG-2, a garnet standard for oxygen isotope ratios: Strategies for high precision and accuracy with laser heating. Geochim Cosmochim Acta 59(24):5223–5231

Walter MJ (1998) Melting of garnet peridotite and the origin of komatiite and depleted lithosphere. J Petrol 39(1):29–60

Wang SJ, Teng FZ, Rudnick RL, Li SG (2015) Magnesium isotope evidence for a recycled origin of cratonic eclogites. Geology 43(12):1071–1074

Winther KT, Newton RC (1991) Experimental melting of hydrous low-K tholeiite: evidence onthe origin of Archaean cratons. Bull Geol Soc Den 39:213–228

Zhang RY, Liou JG (2003) Clinopyroxenite from the Sulu ultrahigh-pressure terrane, eastern China: origin and evolution of garnet exsolution in clinopyroxene. Am Mineral 88:1591–1600

Zhang L, Chen RX, Zheng YF, Hu Z, Yang Y, Xu L (2016) Geochemical constraints on the protoliths of eclogites and blueschists from north Qilian, northern Tibet. Chem Geol 421:26–43